PROTEINS
STRUCTURE ■ FUNCTION ■ BIOINFORMATICS

Molecular mechanism of β-sheet self-organization at water-hydrophobic interfaces

Ana Nikolic,[1,2] Stéphanie Baud,[1,3] Sarah Rauscher,[1,4] and Régis Pomès[1,4]*

[1] Molecular Structure and Function, Hospital for Sick Children, Toronto, Ontario, Canada
[2] Department of Medicine, University of Toronto, Toronto, Ontario, Canada
[3] Laboratoire SiRMa, CNRS UMR MEDyC 6237, IFR 53 Biomolécules, Université Reims Champagne-Ardenne, Reims, France
[4] Department of Biochemistry, University of Toronto, Toronto, Ontario, Canada

ABSTRACT

The capacity to form *β*-sheet structure and to self-organize into amyloid aggregates is a property shared by many proteins. Severe neurodegenerative pathologies such as Alzheimer's disease are thought to involve the interaction of amyloidogenic protein oligomers with neuronal membranes. To understand the experimentally observed catalysis of amyloid formation by lipid membranes and other water-hydrophobic interfaces, we examine the physico-chemical basis of peptide adsorption and aggregation in a model membrane using atomistic molecular simulations. Blocked octapeptides with simple, repetitive sequences, $(Gly\text{-}Ala)_4$, and $(Gly\text{-}Val)_4$, are used as models of *β*-sheet-forming polypeptide chains found in the core of amyloid fibrils. In the presence of an n-octane phase mimicking the core of lipid membranes, the peptides spontaneously partition at the octane-water interface. The adsorption of nonpolar sidechains displaces the peptides' conformational equilibrium from a heterogeneous ensemble characterized by a high degree of structural disorder toward a more ordered ensemble favoring *β*-hairpins and elongated *β*-strands. At the interface, peptides spontaneously aggregate and rapidly evolve *β*-sheet structure on a 10 to 100 ns time scale, while aqueous aggregates remain amorphous. Catalysis of *β*-sheet formation results from the combination of the hydrophobic effect and of reduced conformational entropy of the polypeptide chain. While the former drives interfacial partition and displaces the conformational equilibrium of monomeric peptides, the planar interface further facilitates *β*-sheet organization by increasing peptide concentration and reducing the dimensionality of self-assembly from three to two. These findings suggest a general mechanism for the formation of *β*-sheets on the surface of globular proteins and for amyloid self-organization at hydrophobic interfaces.

Proteins 2011; 79:1–22.

Key words: amyloid; peptide self-aggregation; protein folding; molecular dynamics simulations.

INTRODUCTION

Together with the α-helix, the β-sheet is the most common structural element in proteins. A β-sheet is defined by the lateral association of two or more β-strands whose polypeptidic backbone is nearly stretched, with consecutive side chains extending alternately above and below the mean plane of the backbone ribbon. Despite the common occurrence of β-sheets, the mechanism of β-sheet formation is not fully understood.[1] A major factor underlying this difficulty is that β-sheet propensity depends not only on the nature of the amino acid residue but also on the tertiary context of the polypeptide chain.[2,3] Unlike α-helices, which involve hydrogen bonds between backbone amide groups located four residues apart in the primary polypeptide sequence, the strands of a β-sheet are often connected by nonlocal hydrogen bonds and may even come from different molecules. Importantly, intermolecular β-sheets form the core of amyloid fibrils resulting from the aggregation of misfolded proteins. Amyloid aggregates are associated with severe neurodegenerative diseases, including Alzheimer's (Aβ and Tau proteins), Huntington's (huntingtin), and Parkinson's diseases (α-synuclein).[4,5] Understanding the microscopic forces controlling β-sheet and amyloid formation is an important but largely unresolved task. Here, we use molecular simulations to probe the role of water-hydrophobic interfaces in the self-organization of peptides into β-sheets.

Amyloid fibrils are elongated, insoluble structures found in extracellular plaques.[5] Structural studies have shown that mature amyloid fibrils involve the alignment of short peptide segments, usually between 6 and 12 residues in length, from many protein monomers. Together, these aligned polypeptide stretches form the characteristic core structure of the amyloid fibril, the cross-β sheet, in which β-strands run perpendicular

Additional Supporting Information may be found in the online version of this article.
This work was performed at the Hospital for Sick Children.
Grant sponsor: CIHR; Grant number: MOP84496 PrioNet Canada.
*Correspondence to: Régis Pomès, Molecular Structure and Function, Hospital for Sick Children, 555 University Avenue, Toronto, ON, Canada M5G 1X8
E-mail: pomes@sickkids.ca
Received 6 June 2010; Revised 21 July 2010; Accepted 24 July 2010
Published online 19 August 2010 in Wiley Online Library (wileyonlinelibrary.com).
DOI: 10.1002/prot.22854

to the main axis of the fibril.[6–9] In addition, fragments of many known amyloid disease peptides, including ones from Aβ and α-synuclein, have been shown to adopt this structure, despite vast differences in amino acid sequence.[10] Recent models of IAPP/amylin and α-synuclein suggest that the amyloid forms of these peptides consist of short stretches of β-sheet connected by hairpin loops.[11,12] Crystallographic studies have shown that even 6-residue fragments of various amyloidogenic proteins can adopt a cross-β structure, with sequence-specific differences in packing and register.[10]

The presence of membranes is emerging as an important factor in amyloid formation and toxicity. Amyloidogenic peptides such as Aβ-40 are thought to interact with biological membranes and to modulate membrane properties,[13] either by altering local membrane structure and thickness or via formation of channels or pores.[14] The toxicity of amyloidogenic proteins such as α-synuclein has been associated with binding and permeabilization of liposome vesicles,[15] although some evidence suggests that lipid binding by α-synuclein can inhibit toxicity.[16] Oligomer toxicity has also been demonstrated for short fragments of amyloidogenic peptides, suggesting that it is due to generic structural properties shared by a large number of different sequences.[17] The above evidence suggests that amyloid toxicity is intimately related to the interaction between membranes and oligomers formed in the early stages of amyloidogenesis.

In addition to compromising membrane permeability and inducing cell death, membrane binding by amyloidogenic proteins has also been found to increase the rate of amyloid formation.[18–22] In particular, liposomes with a high content of anionic lipids promote amyloidogenesis in proteins as diverse as insulin, G3P dehydrogenase, myoglobin, a fragment of the immunoglobin light chain, and the Aβ peptide.[13,23–25] Moreover, amyloidogenesis is also catalyzed by reverse micelles[26] and by the hydrophobic surfaces of hexane granules,[27] nonpolar nanoparticles,[28,29] and nonpolar droplets.[30] Finally, the air-water interface has also been shown to promote the self-organization of peptides into β-sheets.[31–34] Together, this evidence suggests that the catalysis of amyloid formation is a generic property of water-hydrophobic interfaces. However, although the effect of surfaces on amyloid formation is well-known and the link between membranes and the toxicity of amyloid diseases is well appreciated, the molecular basis of these phenomena is presently unclear.[14,35]

Elucidating the early stages of peptide aggregation in the presence of a membrane would improve our understanding of the structure and properties of amyloidogenic oligomers and may ultimately provide insight into the molecular basis of their toxicity. As early aggregates are transient and small in size, molecular dynamics (MD) simulation is well-suited for studying the early stages of peptide aggregation and clarifying the role of water-nonpolar interfaces in amyloidogenesis. In recent years, MD simulations at the atomic level of detail have provided insight into the nature and the stability of mature amyloid structure and the formation of small oligomers in water.[36–40] At a lower level of resolution, coarse-grained simulations have shed light on oligomer formation and the nucleation-propagation mechanism of fibrilation suggested by *in vitro* kinetic data.[41–48] Simulations have been performed both on full-length peptides, such as Aβ(1−42), and on short amyloidogenic fragments (e.g.[39,40,49–51]). Nevertheless, extensive conformational sampling of peptides in lipid membranes remains computationally challenging.[52] Although recent simulation studies have begun to examine the interaction of amyloidogenic peptides with membranes or interfaces,[52–61] the aggregation mechanism has not been investigated in atomistic detail.

Here, we use all-atom molecular dynamics simulations to probe the role of water-hydrophobic interfaces in the self-organization of peptides into β-sheets. To achieve statistically meaningful sampling, we study the self-aggregation of short peptides at a model water-hydrophobic interface. The above evidence suggests that short peptides provide suitable models of amyloid formation and toxicity. We focus on two of the simplest and shortest peptides of relevance, namely, $(\text{Gly-Ala})_4$ and $(\text{Gly-Val})_4$, henceforth abbreviated as $(\text{GA})_4$ and $(\text{GV})_4$. GA repeats are known to adopt an extended β-sheet structure in the so-called crystalline domain of many spider silks.[62] The $(\text{GA})_n$ motif is also used in synthetic copolymers, and has been observed to readily form β-sheet-containing fibrils.[63,64] A previous simulation study predicted that an extended $(\text{GV})_n$ repeat has a propensity to form amyloid.[65] To avoid the long relaxation times of atomistic simulations of lipid bilayers, we use an n-octane layer as a simplified model of the nonpolar core of biological membranes. Octane slabs have been shown to be an appropriate membrane mimetic in simulation studies of peptide adsorption and aggregation.[66,67] We investigate the effect of the water-hydrophobic interface on the aggregation of $(\text{GA})_4$ and $(\text{GV})_4$ octapeptides. Specifically, we examine peptide self-assembly successively in water and in the presence of an octane phase. The conformational distribution of peptide monomers and aggregates is characterized. Consistent with experimental evidence, the water-nonpolar interface is found to accelerate β-sheet formation dramatically relative to aqueous aggregates. The physical and molecular basis of catalysis is analyzed and implications to protein folding and amyloid self-organization are discussed.

METHODS

Simulation parameters and protocol

Monomeric and multiple chains of $(\text{GA})_4$ and $(\text{GV})_4$ in water were studied using MD successively with and

without the presence of n-octane. The C and N termini of the peptides were capped with amide and acetyl groups, respectively, to eliminate the effects of terminal charges on aggregation and membrane adsorption. Peptides and octane were modeled using the OPLS-AA force field[68] and the TIP3P model[69] was used for water. All simulations were performed using the GROMACS program, version 3.3.1.[70,71] The simulations were run using the leapfrog Verlet algorithm with a 2 fs integration timestep. Electrostatic interactions were calculated using Particle Mesh Ewald (PME) summation with a grid size of 0.12 nm and a real-space cutoff of 0.9 nm.[72] Lennard-Jones interactions were subjected to twin-range cut-off separations of 0.9 and 1.4 nm. Pressure coupling was semi-isotropic, with a reference pressure of 1 atm, using the Berendsen barostat and a coupling constant of 4 ps, with a fixed z-axis to prevent contraction of the octane layer.[73] Peptide, octane, and water atoms were placed in separate temperature coupling groups, and temperatures were coupled independently with a coupling constant of 0.1 ps. All simulations were run at $T = 298$ K. Covalent bonds containing hydrogen were constrained using LINCS,[74] and the SETTLE algorithm was used for water.[75]

Overall, 126 independent simulations of $(GV)_4$ totaling 8 μs were performed as specified in Table I. The simulations of $(GA)_4$ were subjected to the same protocols unless otherwise noted. The initial conformations of peptide monomers were taken from runs W_M (W'_M for $(GA)_4$) generated in water at 296 K by simulated tempering distributed replica sampling (STDR), a novel generalized-ensemble algorithm developed in our laboratory.[76–78] As in simulated tempering, in STDR replicas undergo a random walk in temperature to enhance conformational sampling. In addition, an extra energy function missing in conventional simulated tempering, the "distributed replica potential energy" (DRPE), enforces the desired distribution of replicas in temperature. The implementation of the STDR method is described in detail elsewhere.[78] The DRPE parameters (c_1 and c_2) both had values of 0.005 for the simulations of the $(GV)_4$ and $(GA)_4$ monomers. The STDR simulations were performed using 35 temperatures distributed exponentially between 230 and 602 K, for a total simulation time summed over all temperatures of 5.5 μs (~150 ns at 296 K). The switch function of GROMACS was used for Lennard-Jones interactions, which corresponds to the usual Lennard-Jones function until 1.3 nm, after which it is switched to reach zero at 1.4 nm. Covalent bonds involving hydrogen atoms were constrained with the SHAKE algorithm.[78] A Fourier spacing of 0.15 nm and fourth-order interpolation were used for PME sums. The real-space Coulombic cutoff was 1.49 nm. Peptide and solvent were coupled to the same reference temperature bath with a time constant of 2 ps using the Nosé-Hoover method.[79,80] All other simulation protocols used in the STDR simulations were the same as those of the canonical MD simulations. A previous STDR study of a similar octapeptide in water showed that this protocol leads to efficient temperature diffusion and adequate convergence of structural properties.[78] The convergence of structural properties of $(GV)_4$ as a function of simulation time at 296 K is shown in Supporting Information Fig. S1.

Table I
List of Simulations of $(GV)_4$ and $(GA)_4$

System	Time (ns/run)	No. of peptides	Octane	Box dimensions (nm)	No. of runs	Concentration (water) (M)	Surface concentration (interface) (M)[a]	Starting state
$(GV)_4$								
A_M[b]	60	2	N	3.59 × 3.59 × 5.5	17	0.0644	0.129	2 monomers in water
O_M	55.8	2	Y	3.59 × 3.59 × 5.5	8	0.0644	0.129	2 monomers in water
O_I	10	8	Y	9.13 × 9.13 × 7.67	43	0.0341	0.080	8 monomers in water
O_{II}	20	8	Y	9.27 × 9.27 × 4.06	43	—	0.080	8 peptides on surface (endpoint of O_I)
O_{III}	82	40	Y	8.30 × 8.30 × 8	1	0.1710	0.482	40 monomers in water[c]
O_{IV}	136	40	Y	8.30 × 8.30 × 8	1	—	0.482	Endpoint of O_{III}
WO	48	16	Y	9.13 × 9.13 × 7.67	3	0.0682	0.160	Conformation from W_I (aggregate of 8) on either side
W_M	150	1	N	3 × 3 × 3	35[d]	—	—	Monomer in water
W_I	20	8	N	9.13 × 9.13 × 4.81	5	0.0331	—	8 monomers in water
W_{II}	160	8	N	5.00 × 5.00 × 5.00	1	0.1062	—	Aggregate (8 peptides) in water
$(GA)_4$								
O'_M	60	2	Y	3.59 × 3.59 × 5.50	12	0.0644	0.129	Monomer in water
O'_I	100	50	Y	9.5 × 9.5 × 6.75	1	0.2453	0.460	50 monomers in water
W'_M	150	1	N	3.00 × 3.00 × 3.00	35[d]	—	—	Monomer in water

[a]Concentration at the water-octane interface is calculated assuming that the z dimension of the interface is about 1 nm—this is the general width of the z value distribution for the center of mass of adsorbed chains.
[b]Simulations performed with an air-water interface.
[c]Run O_{III} was generated by successive additions of 8, 16, and another 16 monomers in water at $t = 0$, 10, and 22 ns, respectively, until all peptides were at the octane-water interface.
[d]Simulated tempering distributed replica sampling (STDR) simulation with 35 replicas at different temperatures.

The octane layer used in simulations O_I-O_{IV} and WO was generated by tiling octane atoms to form a planar phase at the center of the box, and then hydrating the system. The resultant system was energy-minimized and simulated for 600 ps under isotropic pressure coupling. This procedure was sufficient to allow the separation of octane and water into two neat phases and for the octane phase to equilibrate. An air-water interface, used in simulation A_M, was generated by removal of octane molecules from the equilibrated interface of simulation O_M. Simulation A_M was run at constant volume to prevent collapse of the air-water interface. At the starting points of biphasic simulations O_M, O_I, and A_M (see Table I) the peptides were placed in the water phase with their center of mass 2 nm from the interface. In run O_I, the initial separation between peptides on either side of the membrane was ~2.5 nm and the axial separation between the two sets of 4 chains was 5 nm. The resultant systems were energy-minimized and each simulation was run for 400 ps at constant pressure with position restraints on the peptides to allow for solvent equilibration prior to production runs; system composition and production run times are listed in Table I.

To allow peptides to accumulate at the biphasic interface while minimizing spontaneous peptide aggregation in water, in simulation O_{III} additional peptides were introduced into the aqueous solution in three stages, by first adding 8, then 16, then another 16 peptides, allowing them to equilibrate until all peptides had adsorbed at the interface (which took ~10 ns). Analysis of simulation O_{III} was initiated after 32 ns. The initial conformation of simulation W_I was generated by removing the octane from the simulation box and then bringing atoms from the two sides together to fill the gap. The resulting box was approximately equivalent to the water phase of biphasic simulation O_I. In run WO, the aqueous aggregate from run W_I with the most β-sheet structure was added to the aqueous phase on each side of the octane layer used at the start of run O_I.

Analysis

Two distance metrics were computed for the peptides: the distance of the center of mass of the peptide from the octane-water interface along the *z*-axis (a measure of adsorption) and the end-to-end distance, d_{ete}, defined as the three-dimensional Euclidean distance between the first and last C_α atoms of each octapeptide (a measure of extension). To determine the approximate location of the interface, the density of octane was measured in sections along the *z*-axis (the interface normal) and the locations where the density crossed 650 kg/m^3 (i.e., approached the bulk density of n-octane, ~700 kg/m^3) were used as markers for the octane layer.

To compensate for any ruggedness on the octane surface, axial distributions of peptide atoms were generated by computing the distance from the octane-water interface using a Voronoi tessellation-based method similar to that described by Pandit *et al.*[81] The octane C atoms were placed on a two-dimensional grid with 1-nm spacings. The highest and lowest octane C atoms on each point in the grid were then selected and were used to construct the tessellation. This procedure corrects for static and dynamic fluctuations of the octane-water interface compared to calculations in which the axial position of the interface is estimated as a space- and time-averaged position relative to the *z*-position of the center of mass of the octane slab.

Hydrogen bonds were identified as any contact for which putative donor-acceptor and hydrogen-acceptor separations were less than 0.35 and 0.25 nm, respectively, and the donor-H-acceptor angle was greater than 120°. In addition, the DSSP hydrogen-bonding energy criterion was also considered.[82] A bond matches this criterion if its bond energy is ≤ -0.5 kcal/mol. Together, the above criteria defined a hydrogen bond. The secondary structure was analyzed using the DSSP algorithm, excluding the amide and acetyl caps at C and N termini, respectively.[82] The hydration of the peptide backbone was analyzed by calculating the number of hydrogen bonds to water for each amide group (either CO or NH). The hydration of the side chains of $(GV)_4$ was measured as the number of water O atoms within 0.43 nm of each valine C_γ. This value was chosen because it corresponds to the first minimum in the radial distribution function of water oxygen to the C_γ atoms of valine (data not shown), encompassing the first hydration shell around the methyl groups. Various kinetic parameters were calculated by performing least-squares exponential fits of time series to an equation of the form $f(t) = a \times e^{-bt} + c$; error was calculated using the confidence bounds for each parameter obtained by the fitting procedure. Standard error of histograms was calculated using block averaging,[83] with the error bars representing the upper and lower bounds of the 95% confidence interval of the mean.

RESULTS

Summary of simulations

We examined the structure and aggregation of two simple octameric peptides, $(GV)_4$ and $(GA)_4$, successively in water and in the presence of a hydrophobic octane phase. Because the results obtained for $(GA)_4$ are qualitatively similar to those obtained for $(GV)_4$, in this section we present a detailed description of results for $(GV)_4$ and provide numerical values obtained for $(GA)_4$ for the purpose of comparison whenever appropriate. The MD simulations performed on the $(GV)_4$ peptides are summarized in Table I. All the simulations of water and octane resulted in a biphasic system, with neat octane and water phases separated by planar interfaces. In the first series of

simulations, peptide monomers initially placed in water spontaneously diffused to the interface. In simulations O_I-O_{II}, four hydrated peptides diffused to each interface, where the process of self-aggregation initiated. Peptide concentration was then increased from 0.0341*M* to 0.171*M* in 32 ns by adding monomers to the aqueous phase in three installments, allowing them to adsorb at the interface before performing the next addition (simulation O_{III}). This process led to 20 peptides at each interface, where self-aggregation continued freely for another 186 ns (simulations O_{III}-O_{IV}), leading to the spontaneous formation of β-sheets within 218 ns. Control simulations were performed in water (runs W), successively for monomeric peptides (W_M) and for aggregates (W_I and W_{II}). In the later simulations, hydrated peptide monomers organized into amorphous aggregates within a few ns. However, despite rapid aggregation, the emergence of β-sheet structure in the hydrated aggregates was much slower than at the interface. In simulation WO, hydrated aggregates were placed in the presence of an octane phase to study the effect of the hydrophobic interface on the reorganization of amorphous assemblies. Finally, the spontaneous adsorption of $(GV)_4$ monomers at the air-water interface was examined in simulation A_M.

Peptide adsorption to the water-nonpolar interface

All the simulations performed with $(GA)_4$ and $(GV)_4$ in the biphasic solution resulted in the partition of the peptides at the octane-water interface. In Simulations O_M and O_I, $(GV)_4$ peptide monomers initially placed in water bound irreversibly to the planar interface. Adsorption was initiated by interactions between one of the valine side chains and the octane phase [Fig. 1(A)] and usually resulted in the partition of three or four side chains of each monomer into the nonpolar phase [Fig. 1(B)]. Peptide adsorption to the interface occured rapidly, with 99% of all peptide chains bound within 10 ns in simulation O_I. Peptide adsorption follows standard first-order kinetics, with a short relaxation time of 2.30 ns (Fig. S2) reflecting the fact that the 43 simulations of hydrated peptide monomers started with the center of mass of the peptide a mere 20 Å from the biphasic interface. Although the partition of individual valine side chains into the octane phase is dynamic and reversible, peptide desorption was not observed over the time scale of the simulations.

Axial density profiles were computed along the interface normal from the simulations of $(GV)_4$ and $(GA)_4$ monomers (Fig. 2). The peptides distributions peak at the two octane-water interfaces [Fig. 2(A)]. Axial distributions of valine C_γ atoms and of main-chain C_α atoms show that the valine side chains are distributed asymmetrically. The C_γ distribution peaks at the interface and is skewed toward the octane phase, whereas the distribution of C_α atoms in $(GV)_4$ is centered 4 Å above the interface and is more symmetric [Fig. 2(B)]. On

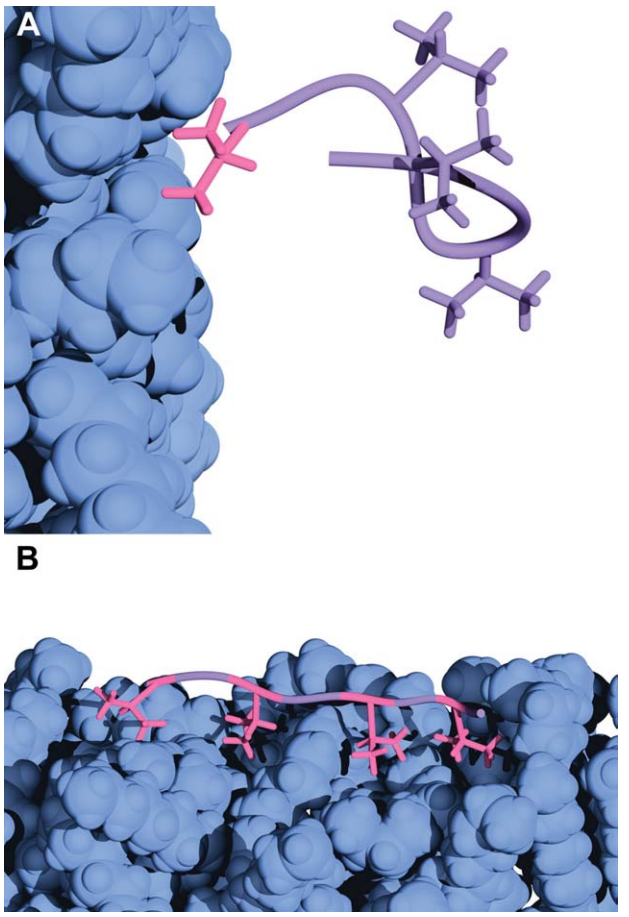

Figure 1

Snapshots showing adsorption of a $(GV)_4$ monomer to the octane surface from simulation O_M. The peptide backbone is represented by a noodle and Val side chains by sticks. **A**: Adsorption is initiated by interaction between at least one valine side chain (pink) and the octane phase (blue) at 1.5 ns. **B**: After 6 ns, the peptide is lying flat on the octane-water interface in an extended conformation.

average, backbone atoms are skewed slightly away from the nonpolar phase compared to C_α atoms [Fig. 2(A)], which is likely due to the polar character of amide groups. The distribution of alanine C_β atoms in $(GA)_4$ is analogous to that of the valine C_γ atoms in $(GV)_4$; however, as a consequence of the shorter alanine side chains, the C_α distribution peaks closer to the surface, at ~2 Å [Fig. 2(B)].

Side chain and backbone dehydration

The above results suggest that peptide adsorption is driven by dehydration of the nonpolar side chains. However, adsorption also results in the partial dehydration of the peptidic backbone. A comparison of side chain and backbone hydration for the various states of $(GV)_4$ is shown in Figure 3. In water, the hydrophobic effect drives self aggregation. Accordingly, average valine side chain hydration, computed as the number of water mole-

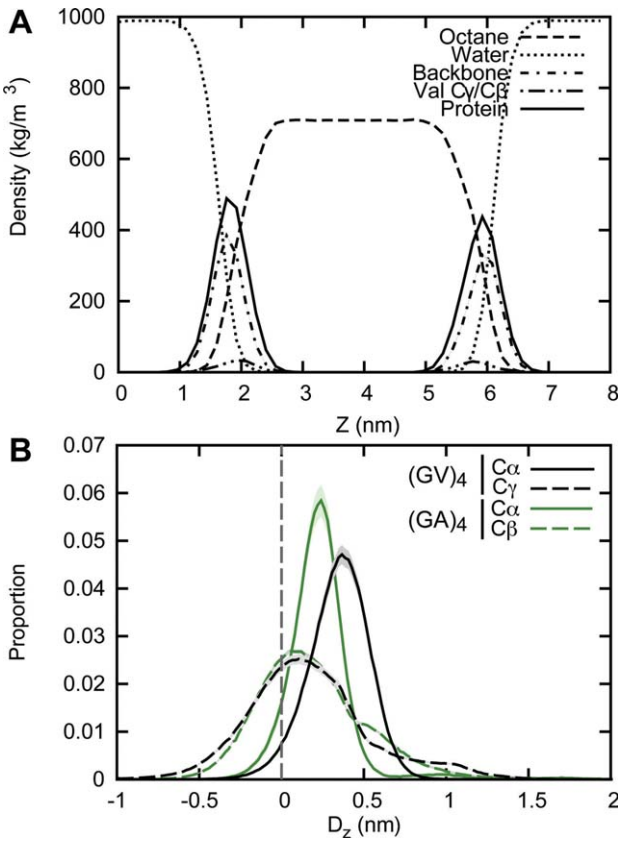

Figure 2

Densities and distributions of peptide atoms relative to the octane-water interface. **A**: Density profile for simulation O_M of $(GV)_4$ showing the distribution of backbone, C_α, and Val C_γ atoms. **B**: Axial distribution of (black) valine C_α atoms and C_γ atoms of $(GV)_4$ and (green) alanine C_α and C_β atoms of $(GA)_4$ normalized with respect to the octane-water interface. These data were compiled from simulations of peptide monomers O_M and O'_M (see Table I).

cules in the first solvation shell of C_γ atoms, drops from 5.5 to 4.6 upon aggregation. Concurrently, the average number of water molecules bound to the peptidic backbone of each octamer drops from 15 to 13.

By contrast, the side chains of adsorbed peptide monomers (O_M) are much less hydrated than those of aqueous aggregates (W_M) and almost as dehydrated as those of mature aggregates (O_{IV}), with 1.6 water molecules per chain on average. These results suggest that the hydrophobic effect is the driving force for the adsorption, but not necessarily the aggregation, of peptides at the water-octane interface. Concurrently, the backbone of adsorbed monomers is partially dehydrated, with an average hydration number of 12 comparable to that of aqueous aggregates. Self-aggregation at the interface is characterized by increasing dehydration of the backbone, to seven water molecules per chain on average (runs O_I through O_{IV}). Initially, two distinct populations corresponding to monomers before and after adsorption differ in both backbone and side chain hydration (run O_I), and the

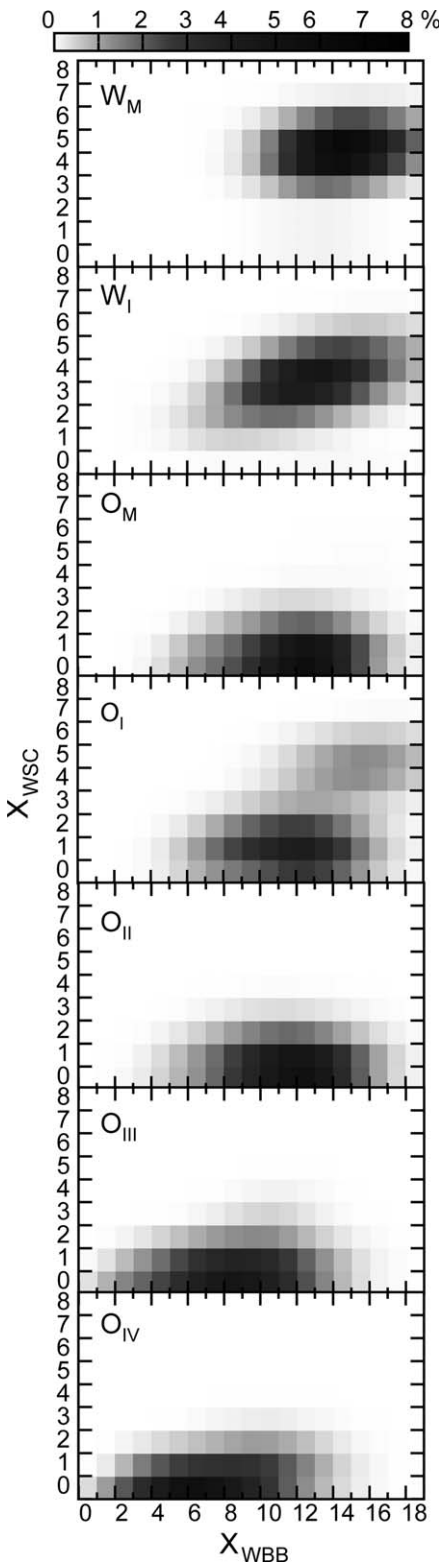

Figure 3

Side chain and backbone hydration of $(GV)_4$. The number of water molecules in the first hydration shell of Val C_γ atoms, X_{WSC}, is compared to the number of backbone-bound water molecules, X_{WBB}, successively for $(GV)_4$ simulations W_M, W_I, O_M, and O_I through O_{IV}.

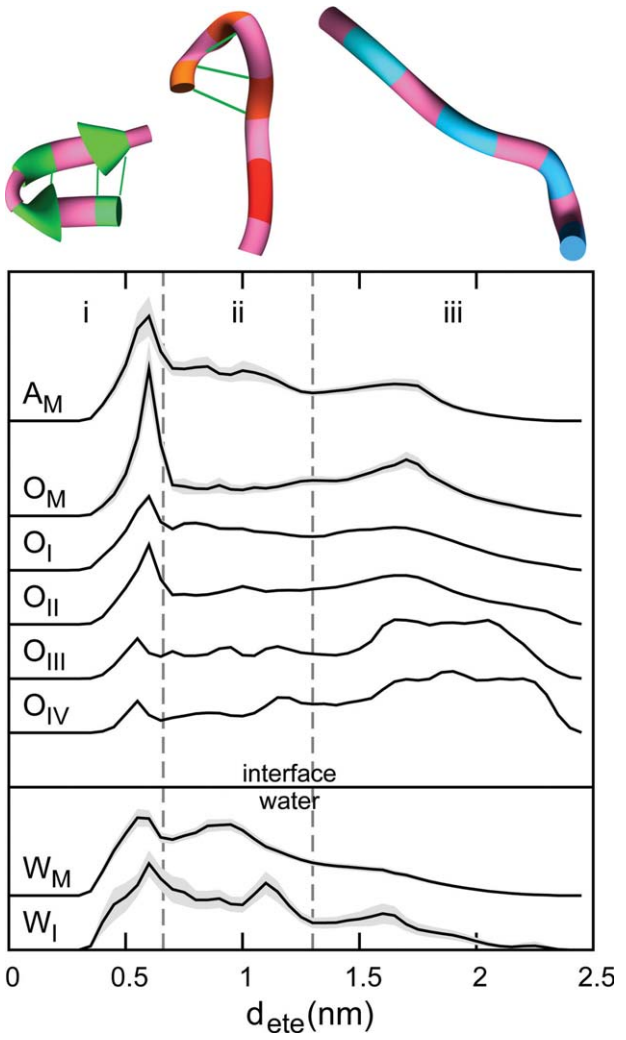

Figure 4

Distribution of end-to-end distances of $(GV)_4$ peptides. **Top:** representative snapshots of the backbone of peptide monomers in (i) short, (ii) intermediate, and (iii) extended conformations. Valine residues are shown in pink and intramolecular hydrogen bonds are shown as green lines. **Bottom:** Normalized distribution of d_{ete}. Biphasic simulations are listed at the top, in order of increasing timescale and concentration. Simulations in water are shown at the bottom. The scale of the *y* axis is arbitrary. Standard error is depicted as gray shading. Dashed vertical lines at d_{ete} = 0.66 and 1.3 nm highlight the boundaries separating conformations (i), (ii), and (iii).

side chains of adsorbed peptides are on average less dehydrated (2.8 water molecules) than those in simulation O_M (1.6) due to shorter simulation times (respectively 10 and 50 ns). This effect is reversed with longer simulation time and higher concentrations. In run O_{II}, all the peptides are adsorbed and their side chains are as dehydrated as those of adsorbed monomers, and the hydration number further drops to 0.9–1.1 in simulations O_{III} and O_{IV}.

The results obtained for $(GA)_4$ are similar with backbone and side chain hydration numbers dropping from 15 to 11 and from 6.6 to 3.2, respectively, upon peptide adsorption at the interface (not shown). This analysis provides quantitative criteria to distinguish between aqueous and adsorbed side chains: all V side chains with a hydration number n_{SC} = 3 and interfacial distance d_Z < 6 Å, and all A side chains with n_{SC} = 5 and d_Z < 4 Å are considered to be adsorbed. These criteria yield equilibrium constants of 5.1 ± 0.8 for valine in $(GV)_4$ and of 2.5 ± 0.2 for alanine in $(GA)_4$, which correspond to free energies of −4.1 ± 0.4 and −2.3 ± 0.2 kJ/mol for the transfer of individual V and A side chains from water to n-octane. The corresponding adsorption probabilities of 84% and 70% explain why peptide desorption, which requires hydration of all four side chains, is unlikely.

Adsorption displaces the conformational equilibrium of the peptides

Both in water and at the interface, $(GV)_4$ and $(GA)_4$ monomers are conformationally disordered: they adopt many different conformations which interconvert over the course of the simulations. Accordingly, we use a global structural property, the distribution of the end-to-end distance, d_{ete}, to represent this conformational equilibrium. The comparison of results obtained for aqueous and adsorbed $(GV)_4$ peptide monomers reveals essential differences (Fig. 4). First, the end-to-end distribution is significantly sharper for adsorbed peptides than their hydrated counterpart at short extensions. In addition, it contains a peak in the long range which is absent in the aqueous case. Inversely, conformations corresponding to intermediate extensions are more populated in water than at the interface. We define three conformation types based on the two intersections between hydrated and interfacial distributions: (i) short for d_{ete} < 0.66 nm; (ii) medium-length for 0.66 < d_{ete} < 1.3 nm; and (iii) long for d_{ete} < 1.3 nm. Representative conformers of all three categories of adsorbed $(GV)_4$ are shown in Figure 4 and the populations of all three states are listed in Table II. Those with a small d_{ete} (left) include β-hairpin-like conformations, although they do not always contain intramolecular hydrogen bonds. Those with intermediate d_{ete} adopt diverse conformations, including hydrogen-bonded turns and conformations devoid of intramolecular hydrogen bonds. Finally, the stretched, strand-like conforma-

Table II

Fractional Population of Different Conformations of $(GV)_4$

	(i) d_{ete}<0.66 nm	(ii) 0.66≤d_{ete}≤1.3 nm	(iii) d_{ete}>1.3 nm
O_M	0.30 ± 0.03	0.26 ± 0.03	0.44 ± 0.04
O_I	0.19 ± 0.01	0.38 ± 0.01	0.42 ± 0.01
O_{II}	0.18 ± 0.01	0.32 ± 0.01	0.50 ± 0.01
O_{III}	0.10 ± 0.01	0.26 ± 0.01	0.65 ± 0.01
O_{IV}	0.06 ± 0.01	0.22 ± 0.01	0.71 ± 0.01
W_M	0.26 ± 0.02	0.53 ± 0.02	0.22 ± 0.01
W_I	0.26 ± 0.03	0.48 ± 0.04	0.26 ± 0.04

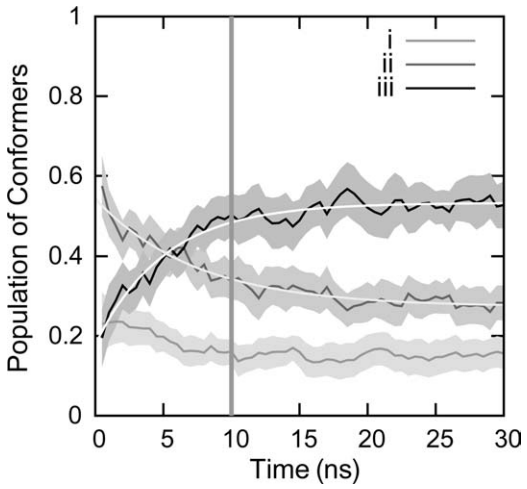

Figure 5

Time-evolution of the relative population of (i) short, (ii) intermediate, and (iii) extended $(GV)_4$ conformers in simulations O_I-O_{II}. Significant peptide extension occurs in the first 10 ns, primarily at the expense of intermediate-length conformations. The curves of best fit for extended and intermediate conformer populations (white lines) are $f(t) = 0.533-0.354\ e^{-0.198t}$ and $f(t) = 0.273 + 0.270\ e^{-0.135t}$, with relaxation times of 5 and 7.4 ns, respectively.

tions always lack hydrogen bonds. Thus, the adsorption of peptides at the octane/water interface profoundly displaces the conformational equilibrium in favor of stretched conformers resembling β-hairpins and β-strands. A similar effect, albeit not quite as pronounced, is also apparent at the air-water interface (simulation A_M).

Self aggregation at the water-octane interface further displaces the conformational equilibrium of the peptides (Fig. 4, Table II). The magnitude of the peak and the population of peptides at short extensions decrease dramatically from simulations O_M and O_I through O_{IV} as the concentration and time spent on the interface increase. Concurrently, the population of extended conformations grows, suggesting that hairpin-like conformations are gradually replaced by extended ones. In contrast, aqueous peptides retain a proportion of closed conformations similar to that of adsorbed monomers regardless of their aggregation state. Furthermore, they rarely occupy extended conformations, and remain intermediate in length even after self aggregation. The ruggedness in the conformational distribution for run W_I is due in part to the slow rate of conformational reorganization of the peptides in aqueous aggregates.

Together, these results show that the conversion of intermediate conformers to extended ones is a consequence of $(GV)_4$ adsorption that is observed neither in monomers nor aggregates in water. In run O_{IV}, nearly three-quarters of the chains are in extended conformations, a three-fold increase compared to aqueous monomers. The time evolution of short, intermediate, and extended peptide populations in runs O_I and O_{II} is shown in Figure 5. The increase in the population of extended states occurs exponentially, with a relaxation time of 7.4 ns, primarily via conversion of intermediate-length conformers. By contrast, the population of short, hairpin-like conformers decays more slowly with time. Although the direct conversion from short to extended forms may occur, this process is more likely to take place in two stages involving conformers of intermediate length.

Aggregation and hydrogen bonding

The time evolution of the fraction of peptides aggregated, as defined by the presence of at least one intermolecular peptide–peptide hydrogen bond, is shown in Figure S3. At the interface, the rate of aggregation follows simple exponential kinetics with a relaxation time of 6.4 ns at a concentration of 0.033*M* (run O_{II}). Aggregation was 55%-complete by the end of simulation O_{II} and 99%-complete by the end of simulation O_{IV} (similarly, it was 96%-complete by the end of $(GA)_4$ simulation O'_{II}). Self-aggregation led to a rapid increase in the number of peptide–peptide hydrogen bonds (Fig. 6). In runs O_I-O_{II}, the number of intermolecular hydrogen bonds grew exponentially to over 1.5 bonds per chain (i.e., about 3 per aggregated chain) within 30 ns, while the number of intramolecular hydrogen bonds remained approximately constant at 0.6 [Fig. 6(A)]. At higher concentration, the total number of hydrogen bonds approached an asymptotic value of 7.70 per chain within 200 ns, while the number of intramolecular hydrogen bonds decreased slowly as the peptides formed ordered aggregates at the interface [Fig. 6(B)]. By contrast, the average number of intramolecular hydrogen bonds in aqueous monomers was significantly larger than at the interface (0.9 vs. 0.6) and remained relatively large in aqueous assemblies.

In water, the peptides clustered into largely-amorphous globular aggregates. The eight monomers rapidly formed hydrogen-bonded dimers and trimers, even reaching a single aggregate in three of five 20-ns simulations (run W_I). In contrast, 45% of peptide chains remained monomeric after 30 ns at the interface in (run O_{II}). The initial rate of hydrogen-bond formation was higher in aqueous aggregates than at the interface [Fig. 6(C)]. This burst coincided with the initial collapse into clusters in the first 15 ns, after which hydrogen bonding increased at a lower rate through rearrangements within existing aggregates. In simulation W_{II}, the number of hydrogen bonds per monomer rose to 5 in the first 10 ns and remained constant for the rest of the simulation, with the exception of a 20-ns spike where a large number of intermolecular hydrogen bonds were transiently formed and dissociated [Fig. 6(D)]. The fact that the number of intermolecular peptide–peptide hydrogen bonds formed at the interface reaches a plateau in both low- and high-concentration simulations [Figs. 6(A,B)] is a consequence of both aggregation and self-organization. At lower concentra-

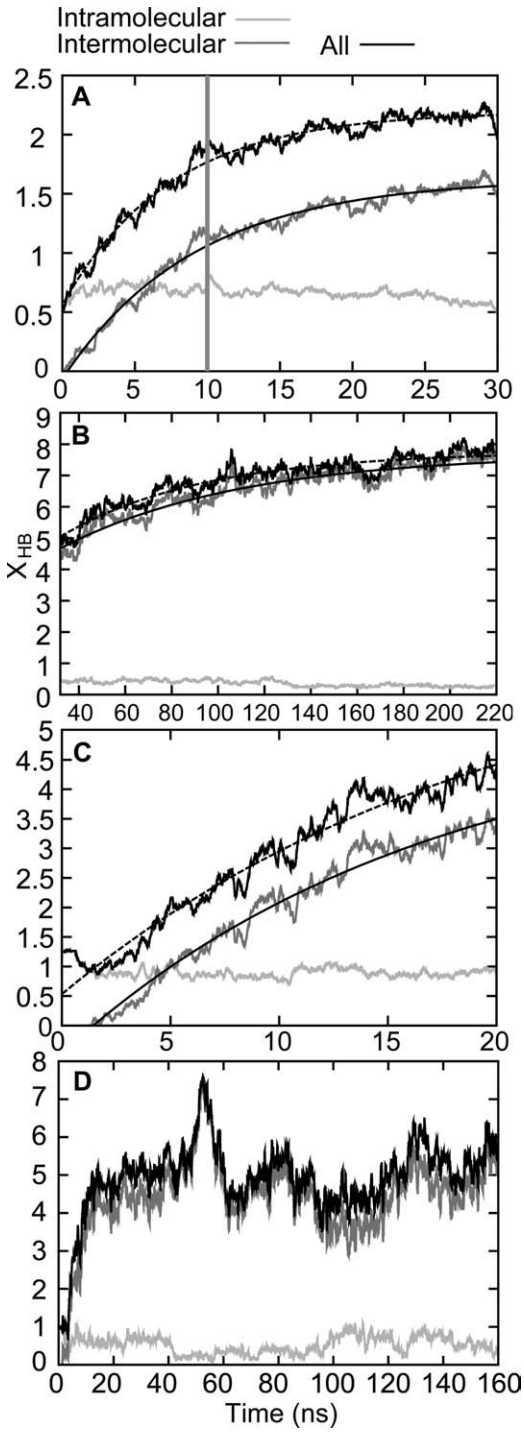

Figure 6

Time evolution of the number of peptide–peptide hydrogen bonds per monomer in simulations of aggregates. **A**: Simulations O_I and O_{II}. Fit for intermolecular bonds: $f(t) = 1.630-1.696e^{-0.109t}$. Fit for all bonds: $f(t) = 2.194-1.635e^{-0.135t}$. **B**: Simulations O_{III} and O_{IV}. Fit for intermolecular bonds: $f(t) = 7.700-4.561e^{-0.013t}$. Fit for all bonds: $f(t) = 7.759-4.564\ e^{-0.016t}$. **C**: Simulation W_I. Fit for intermolecular bonds: $f(t) = 5.252-5.721e^{-0.059t}$. Fit for all bonds: $f(t) = 6.691-6.159e^{-0.050t}$. **D**: Simulation W_{II}.

tions, the peptides take longer to diffuse and bind to each other. Once the chains aggregate, they become trapped in local energy minima and must undergo rearrangement to gain additional hydrogen bonds. In water, this reorganization process is further impeded by a greater conformational heterogeneity.

To characterize the conformational dependence of hydrogen-bond formation, we recomputed the end-to-end distance distributions separately for four mutually exclusive categories corresponding to peptides forming either inter- or intramolecular hydrogen bonds, both, or neither (Fig. 7). At the interface, these four classes separate into two groups: the degree of peptide extension is

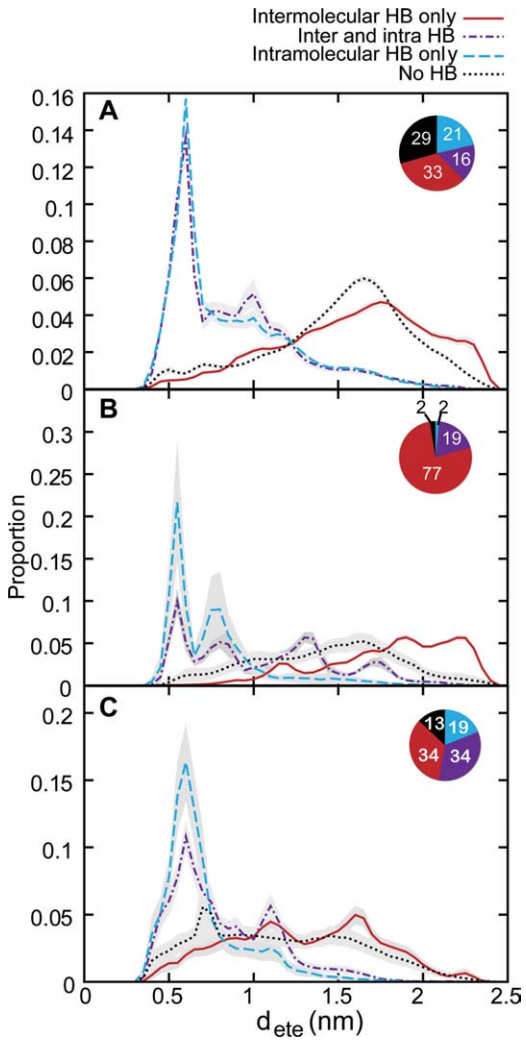

Figure 7

End-to-end distance distribution for different hydrogen-bonding classes of $(GV)_4$ peptides. **A**: Simulation O_{II}. **B**: Simulation O_{IV}. **C**: Simulation W_{II}. Standard error is represented by shading. Pie chart insets indicate the relative populations (in %) of the four different classes. Red: Intermolecular hydrogen bonds only; purple: inter and intramolecular hydrogen bonds; blue: intramolecular hydrogen bonds only; black: no hydrogen bond.

essentially determined by the presence of intramolecular hydrogen bonding. The two conformational classes devoid of intramolecular hydrogen bonds correspond to the extended portion of the d_{ete} range, with the longest extensions reserved to peptides containing only intermolecular bonds [Figs. 7(A,B)]. The striking emergence of the pronounced shoulder at $d_{ete} > 2$ nm in simulations O_{III}-O_{IV} reflects the extension of β-strands in newly formed β-sheets. In contrast, the two conformational classes containing intramolecular bonds exhibit similar distributions and prevail in the short d_{ete} range, which reflects the dominant contribution of hairpin-like conformations to these two populations. The two distributions eventually diverge (in simulations O_{III}-O_{IV}) due to the gradual extension induced by intermolecular hydrogen bonds, suggesting that peptides containing both inter and intramolecular hydrogen bonds can act as intermediates in the formation of β-sheets. Qualitatively, a similar behavior is observed in aqueous aggregates, although the peptides lacking intramolecular hydrogen bonding are significantly less extended than at the interface.

The proportion of peptides in each category also varies with the systems: as shown in the insets of Figure 7, on average half of the peptides are aggregated in run O_{II}, 1/3 of which contain intramolecular hydrogen bonds, while 96% of the chains in O_{IV} are aggregated, 1/5 of which also have intramolecular bonds. The fraction of peptides with both intra and intermolecular hydrogen bonds increases from simulation O_I to O_{III}, then drops off as aggregates mature in simulation O_{IV} (not shown), confirming that the peptides containing both types of hydrogen bonds act as intermediates in the process of self-organization. In contrast, half of the 68% of peptides that have aggregated in simulation W_I also form intramolecular hydrogen bonds, reflecting the greater conformational heterogeneity of aqueous aggregates relative to their adsorbed counterparts.

To examine the interplay of backbone desolvation and self-organization, the distribution of backbone-water hydrogen bonds is shown as a function of the number of peptide–peptide hydrogen bonds (Fig. 8). The anticorrelation between these two variables reflects the progressive replacement of solvent by peptide hydrogen bonds from simulations O_I through O_{IV} as aggregation and self-organization proceed. The overall trend is a gradual increase in the number of peptide–peptide hydrogen bonds and in the spread of the distribution, which rises from between 0 and 4 in simulation O_I to between 4 and 12 in O_{IV}. The same analysis for simulation W_I shows results similar to simulations O_I-O_{II}, albeit with a higher degree of backbone hydration. Although the slope of the 2D distribution is $\sim -3/5$ and $-2/3$ in run O_I and W_I, it approaches -1 in runs O_{II}-O_{IV}. Thus, although backbone dehydration is undercompensated by peptide–peptide hydrogen bonds upon initial adsorption of monomeric peptides and at early stages of aqueous aggregation, inter-

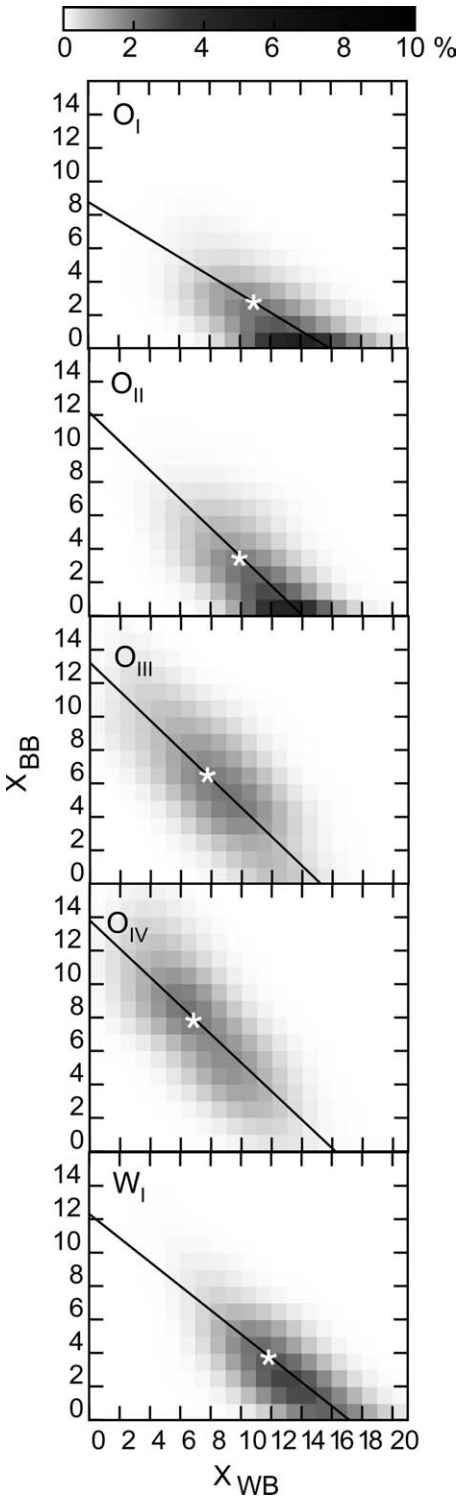

Figure 8

Distributions of the number of backbone–backbone hydrogen bonds per $(GV)_4$ monomer, X_{BB}, vs. the number of water molecules hydrogen bonded to the backbone, X_{WB}. Results are shown successively for simulations O_I through O_{IV} and W_I. The average is shown as a white star and a linear fit is shown as a black line.

molecular peptide hydrogen bonds nearly make up for it during self-organization at the interface. These findings suggest that peptide–peptide hydrogen bonding drives the emergence of secondary structure at the interface. Compared to its monomeric counterpart, the peptidic backbone is on average 12% and 37% dehydrated in aggregates formed in water and at the interface, respectively.

Self-organization into β-sheets

To characterize the time dependence of self-organization, the secondary structure of the aggregates is shown in Figure 9. The amount of β-sheet structure grows monotonically in runs O_I through O_{IV}, with the fraction of residues forming β-sheets increasing from 0 to 4, 6, 10%, and up to nearly 30% after 218 ns of simulation. By contrast, the fraction of β-bridges, which are defined as short β-sheet-like segments of two residues in length, remains near 5% of all residues in all simulations. Since β-sheets are extended β-bridges (as they involve more than two residues), these findings suggest that β-bridges act as substrates for the formation of β-sheets. Moreover, the combined population of all other hydrogen-bonded structures (including turns and helical conformations) in simulations O_{II} through O_{IV} is less than 5%. The trend was similar for $(GA)_4$ peptides, although comparatively less β-sheet structure, 11%, was formed after 100 ns (not shown). By contrast, although the amount of β-sheet structure in aqueous aggregates of $(GV)_4$ (runs $W_{I\text{-}II}$) is comparable to that at the interface at early stages of aggregation (12% for O_I vs. 9% for W_I), it increases slowly and nonmonotonically, with dramatic fluctuations in the 100-ns time range [W_{II}, Fig. 9(D)]. Despite the higher rate of aggregation, self-organization merely reaches 12% after 160 ns vs. 30% at the interface over the same time scale. These differences reflect more disordered initial conformations, as a result of which the formation of β-sheets requires considerably more reorganization in water than at the interface. Accordingly, β-bridges make up a large fraction of β structure in aqueous aggregates, even at long times. The sharp but transient increase in β-sheet content at $t \sim 50$ ns [Fig 9(D)] corresponds to the spike noted in Figure 6(D).

The final structure of peptide aggregates on each of the two interfaces at $t = 218$ ns is depicted in Figures 10 and 11, while snapshots from early stages of self-aggregation are depicted in Figure S4 for comparison. Whereas a few β-hairpins and short β-sheet segments are apparent at early stages, after 218 ns the majority of peptides take part in β-sheets involving two or more residues per chain (Fig. 10). Ordered aggregates include several trimers and tetramers, some of which appear to be in the process of merging [Fig. 11(top)]. The aggregates contain both parallel and antiparallel β-sheets at various stages of registration. In water, the largest extent of contiguous secondary structure consists primarily of an extended β-sheet dimer [see Fig. 12(A)]. Nevertheless, this transient structure is

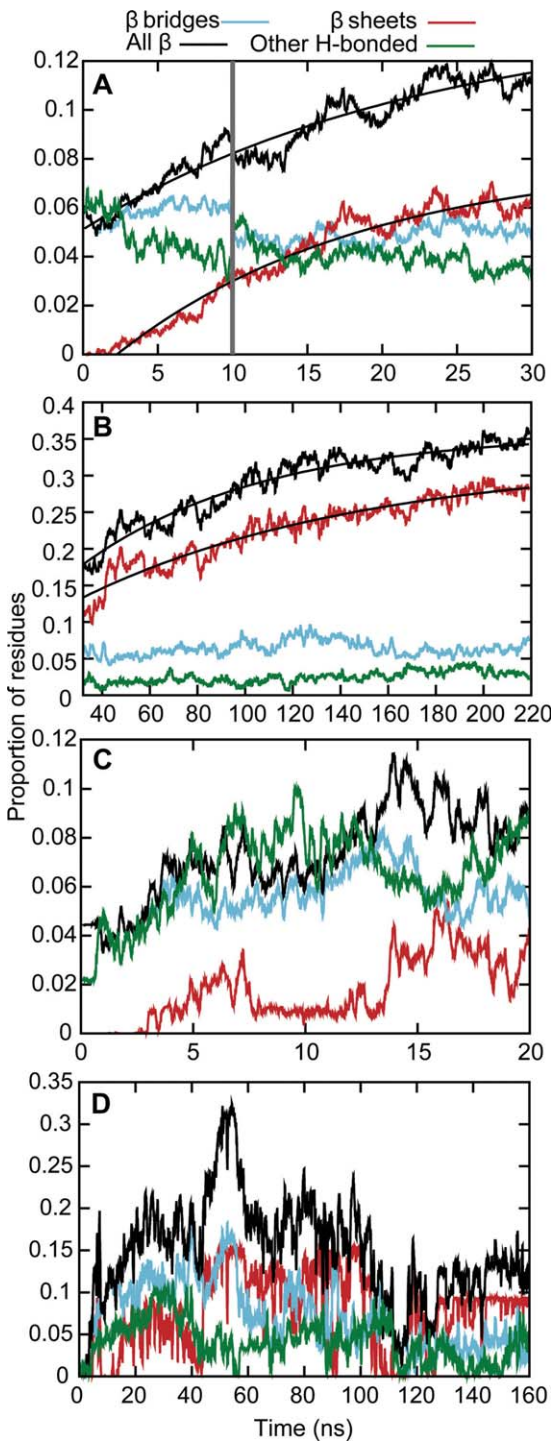

Figure 9

Time evolution of secondary structure in $(GV)_4$ aggregates at the octane-water interface and in aqueous solution. **A**: Simulations O_I and O_{II}. Fit for β sheets: $f(t) = 0.0827 - 0.0928e^{-0.0564t}$. Fit for all β: $f(t) = 0.139 - 0.0880e^{-0.0436t}$. **B**: Simulations O_{III} and O_{IV}. Fit for β sheets: $f(t) = 0.322 - 0.247e^{-0.00849t}$. Fit for all β: $f(t) = 0.358 - 0.274e^{-0.0132t}$. **C**: Simulation W_I. **D**: Simulation W_{II}.

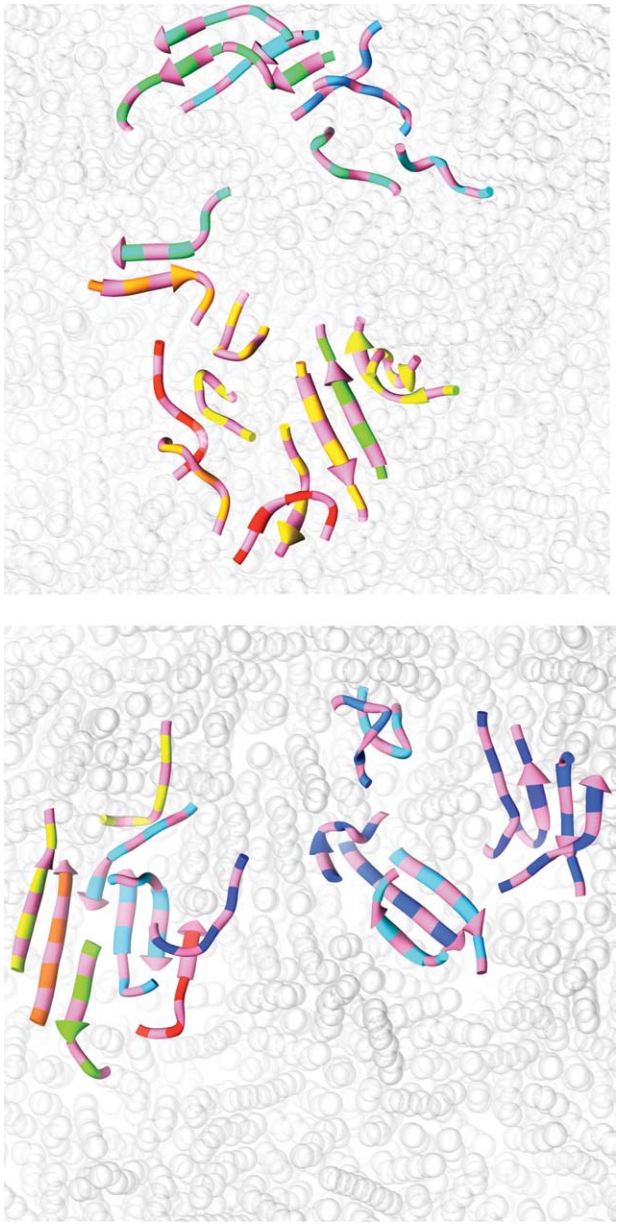

Figure 10

Snapshots of $(GV)_4$ aggregates at the two octane-water interfaces at the end of simulation O_{IV} (t = 219 ns). Both sides show extended dimers, trimers, and larger structures. The octane surface is shown in gray. The peptides are shown with valine residues in pink and glycine residues in a different color depending on the chain. B-sheets are represented as flat arrows. Both interfaces contain dimers and aggregates of higher order, with both parallel and antiparallel β-sheets at various degrees of registration.

globally disordered. Although elongated β-sheet structure is attained at the interface, it should be noted that even adsorbed peptides are still largely disordered (60 to 70% in O_{IV}, higher in the other runs), as is apparent from the structural detail shown in Figure 11. The role of Val side chain adsorption in self-organization is evident from the perspective in Figure 11(middle), while the side-view shown in Figure 11(bottom) emphasizes at once the approximate two-dimensional nature of the aggregates and the partial hydration of the backbone.

The prevalence of disordered states implies that significantly more time is required to reach a fully ordered state. The number of hydrogen bonds depends on concentration, the progress of the aggregation, and the total number of chains. The largest β-sheet that a tetrameric aggregate of octapeptides can form contains $(2\times8+2\times8+8+8)/4 = 12$ hydrogen bonds per chain due to finite size. This theoretical maximum rises to 15.2 with 20 peptides per interface (simulations O_{III}-O_{IV}) and

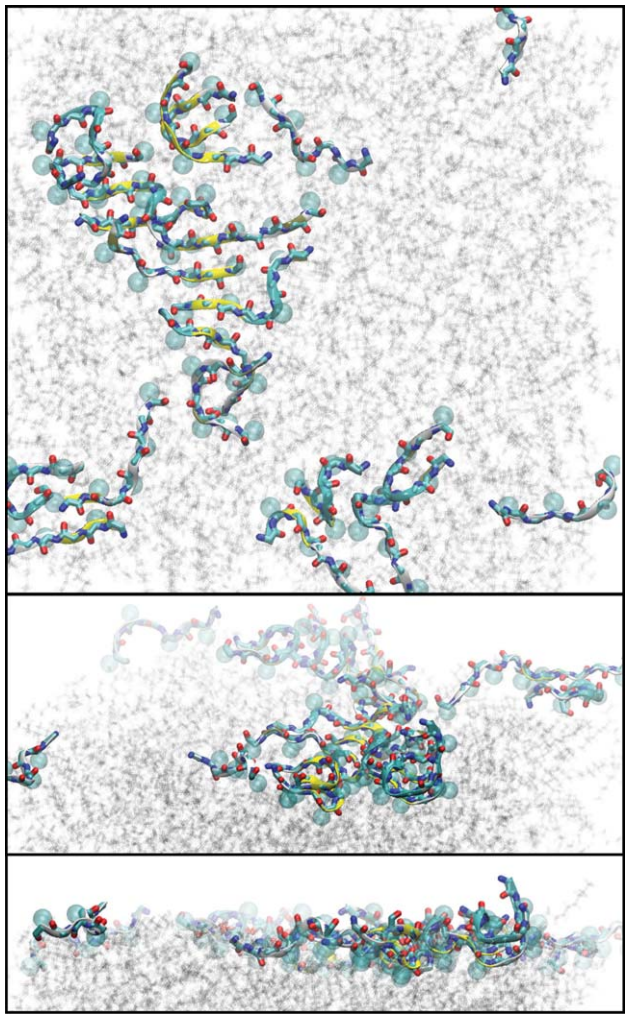

Figure 11

Self-organization at the interface. Views of $(GV)_4$ aggregates after 219 ns (simulation O_{IV}). B-sheets are shown in yellow and octane is shown in gray; water is omitted and valine side chains are shown as single spheres for clarity. **Top**: Top view emphasizing secondary-structure formation. **Middle**: Side view highlighting side-chain adsorption and showing that despite self-organization, many peptide chains are still partially adsorbed and significantly disordered. **Bottom**: Side view emphasizing the two-dimensional character of the aggregates.

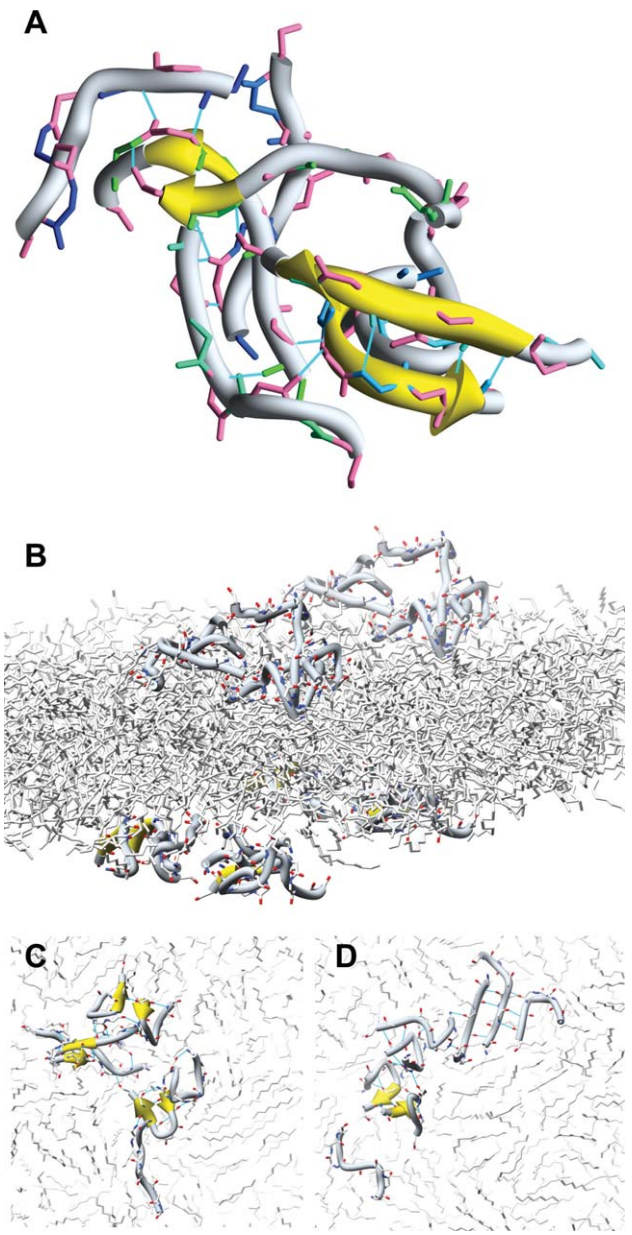

Figure 12

Self-organization in aqueous and adsorbed aggregates. **A**: Most extensive β-sheet conformation from simulation W_{II}. This conformation corresponds to the peak occuring at $t \sim 50$ ns, as noted in Figures 6(D) and 9(D) (see text). Different colors are used for the glycine residues of different peptide chains. Peptide–peptide hydrogen bonds are shown as blue lines. **B**: Intermediate conformation of simulation WO following adsorption of two aqueous aggregates on either side of the octane phase. **C**,**D**: Final conformation of peptide aggregates at the two octane-water interfaces in simulation WO. Peptide–peptide hydrogen bonds are shown as lines.

16 for an infinite sheet. As only a small fraction of the chains in simulations O_I-O_{II} are aggregated, normalizing the number of observed hydrogen bonds by the fraction of chains aggregated yields an average of three hydrogen bonds per bonded chain, which corresponds to 12, 19, and 37% of the theoretical maximum for tetramers, trimers, and dimers, respectively. Considering that the early aggregates consist mostly of dimers, such an extent of self-organization is substantial considering the short time scale of these simulations. Similarly, in simulations O_{III}-O_{IV}, with 20 peptides on each surface, the maximum number of bonds formed is approximately seven bonds per chain, which is corroborated by the observation of a fully formed dimer (maximum of eight hydrogen bonds) and of partly ordered trimers and tetramers (maximum of 10 or 12 hydrogen bonds) [see Fig. 11(top)].

Reorganization of preformed aggregates

Although the results presented above pertain to self-aggregation in water and at the interface, respectively, it is also possible that, due to the high rate of aggregation of peptides in water, aggregates form prior to peptide adsorption on the interface. To probe the competition between the forces driving peptide aggregation, membrane adsorption, and conformational reorganization, we performed a series of additional simulations in which several states of the preformed aqueous aggregate of 8 $(GV)_4$ peptides from simulation W_{II} were placed in the presence of an octane phase (simulation WO). This procedure led to the remarkably rapid adsorption of the amorphous aggregates, with half of the valine side chains partitioning into the octane phase within the first 2 ns of simulation (Fig. 13, top). In the subsequent 45 ns, valine adsorption only increased by 25%, whereas the amount of β-sheet more than doubled, increasing in several bursts from 12 to 28% (Fig. 13, bottom). The final conformation of peptide aggregates in one of the three WO simulations is shown in Figure 12(B–D). The topology of these aggregates is nearly two-dimensional as previously obtained by diffusion of monomers at the interface (see Fig. 11). Surface adsorption breaks down the amorphous aggregate and drives the spread and subsequent self-organization of the peptides. The dramatic acceleration of β-sheet self-organization following surface adsorption of the preformed aggregate demonstrates that the phase separation of nonpolar side chains is strong enough to trigger not only the adsorption and preorganization of peptide monomers, but also the adsorption and the reorganization of an amorphous aqueous aggregate. The latter effect is consistent with the former mechanism but with the replacement of the surface diffusion step by a rapid change in the morphology of the three-dimensional aggregate. These results suggest that at high aqueous concentrations, the peptides are likely to aggregate via 3D diffusion in water and reorganize at the interface, whereas the lower concentration limit may favor initial adsorption of monomers followed by preorganization and comparatively slow 2D diffusion at the interface.

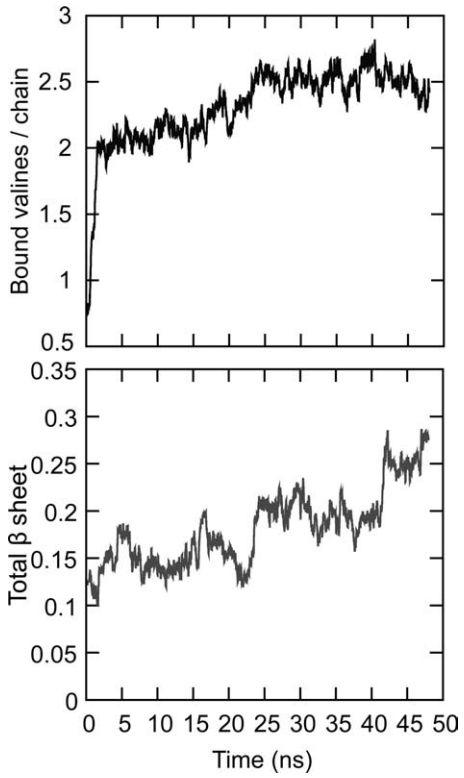

Figure 13

Surface-induced reorganization of aqueous aggregate in simulation WO. **Top**: Number of Val side chains adsorbed. **Bottom**: Fraction of peptide groups forming β-sheet structure.

DISCUSSION

The above results paint a picture of β-sheet formation at water-hydrophobic interfaces which is fundamentally different from that in water. In this section, we analyze the thermodynamic and kinetic basis of self-organization and we discuss the implications of our findings to amyloid formation and protein folding.

Structural and physical basis of peptide self-organization

The phase separation of nonpolar side chains is the initial event that results in diverging pathways of aggregation in water and in the biphasic system. While the hydrophobic effect is the primary driving force for peptide aggregation in water, in the biphasic systems the same effect instead drives the partition of nonpolar side chains into the nonpolar (octane) phase. The transfer free energies of Val and Ala side chains from water to the octane interface, as computed from our simulations, are −4.07 and −2.29 kJ/mol, respectively. These values are close to the transfer free energy of Val and Ala side chains from water to octanol of −4.93 and −2.17 kJ/mol, respectively.[84] In a recent simulation study, the good overall agreement between the computed partition of amino-acid side chain analogues from water to the surface of lipid bilayers[85] and measured partition coefficients for transfer from water to octanol[84,86] was taken as a confirmation that octanol is a good mimetic of the lipid membrane interface.[85] In turn, the fact that our results are also in good agreement with the octanol scale suggests that the water-octane interface is a good mimetic of the water-lipid interface, at least as far as hydrophobic side chains are concerned.

In addition, the quantitative agreement between side-chain partition in our octapeptides, which contain four hydrophobic side chains, and the results of studies using pentapeptides as hosts[86] or small-molecule analogues of amino-acid side chains[85] suggests that the adsoprtion of individual side chains to the hydrophobic interface occurs independently of the rest of the peptide. This observation has two implications: first, it indicates that intramolecular interactions between side chains do not play a significant role in the separation. Second, it implies that the polypeptide backbone is passive in the adsorption process, as also suggested by our finding that the proximity of the backbone to the surface is dictated by the length of the adsorbed side chains [see Fig. 2(B)].

Accordingly, adsorption has profound effects on the structure and hydration of the peptide. Binding to the interface decreases the conformational freedom of the polypeptide chain and shifts its conformational equilibrium from highly disordered to locally extended microstates, with amide planes lying approximately parallel to the interface. The conformational ensemble of the adsorbed peptide monomers is displaced toward a bimodal distribution favoring closed, hairpin-like conformations and elongated, strand-like conformations (Fig. 4). This effect is a direct consequence of hydrophobic partition in the peptide sequences considered, in which the side chain of every other residue is nonpolar. Both hairpin-like and extended conformations satisfy the partition of these residues. Although Gly is considered nonpolar, its lack of a side chain results in a weak propensity to partition into the nonpolar octane phase relative to V and A. As a result, $(GA)_n$ and $(GV)_n$ peptides behave like binary amphipathic sequences. It is the propensity for alternating residues to face the octane5 phase that drives local elongation of the backbone. In turn, the resulting conformational restriction of the backbone torsions to the β-sheet basin determines the formation of sheet-like secondary structure upon aggregation [see Figs. 11 and 13(bottom)].

Although surface adsorption reduces the conformational freedom of the peptides, this effect does not in itself lead to their aggregation. Rather, it is the partial dehydration of the backbone, as it lies on the interface that drives the formation of peptide–peptide hydrogen bonds. In the monomeric state, the average number of water molecules bound to the peptide decreases from

about 15 to about 12 upon adsorption in $(GV)_4$ (Fig. 3) and from 15 to 11 in $(GA)_4$. The propensity to compensate by forming peptide–peptide hydrogen bonds is manifested by the formation of β-hairpins, which is the only way to combine local extension of the backone and intramolecular hydrogen bonding. By contrast, in the presence of other peptides, the number of peptide–peptide hydrogen bonds is maximized by making intermolecular β-sheets. As a result, the formation of intermolecular hydrogen bonds drives aggregation and further displaces the bimodal conformational equilibrium of the peptide backbone toward fully elongated conformations (Fig. 4). Self-organization proceeds via monotonic increases in both hydrogen-bonding and β-sheet content (Figs. 6 and 9) which coincide with further backbone desolvation (Fig. 8).

The process described above highlights two types of entropic contributions, (i) the dehydration of nonpolar side chains, which is thermodynamically favorable (since it corresponds to a positive change in entropy), and (ii) one of its consequences, the reduction of the internal conformational freedom of the peptide main chain, which is unfavorable entropically and ultimately promotes the ordering of peptide aggregates via the formation of β-sheets. In addition, entropic factors contributing to the catalysis of β-sheet formation at the interface also include (iii) the restriction in orientational freedom resulting from peptide adsorption, which replaces a three-dimensional process of self-assembly by a two-dimensional one, further decreasing the likelihood of forming disordered aggregates such as those observed in water. Finally, adsorption also results in (iv) an increase in the local concentration of the peptide, as the same number of monomers is found near a two-dimensional surface rather than in a three-dimensional volume. While the magnitude of this effect depends on the surface-to-volume ratio, the relative confinement of peptide monomers displaces the aggregation equilibrium toward the aggregated state,[35] as also suggested in recent coarse-grained simulation studies of amyloid aggregation on the surface of lipid vesicles[87] and nanoparticles.[88]

This process is fundamentally different from the formation of amyloid in the aqueous phase for several key reasons. First, as mentioned above, aggregation in water is driven by the hydrophobic effect, not by backbone dehydration. Second, the three other entropic factors promoting β-sheet formation at the interface (namely, increase in concentration and loss of orientational and conformational freedom) are missing in the process of aqueous aggregation. Ultimately, the reason why the interface promotes β-sheet formation is that its biphasic nature and two-dimensional character complement those of β-sheets. As a result, when monomers self-aggregate at the interface, they are already largely preordered, contrary to their disordered state in water. In other words, the (entropic) catalysis of β-sheet self-organization by the water-hydrophobic interface results from the provision of a template whose two-dimensional topology and physical properties match those of amphipathic β-sheets.

Mechanism and kinetics of β-sheet formation

The different pathways of self-organization lead to radically different kinetic properties. Our results in water are compatible with kinetic models of amyloid formation in aqueous solutions. The latter process is usually described as a nucleation-propagation mechanism, in which an initial lag phase corresponds to the formation of a thermodynamically unfavored intermediate state, the nucleus, followed by the favorable addition of monomers resulting in the rapid elongation of the proto-fibrillar aggregate.[35,89,90] Although our simulations of aqueous aggregates did not lead to the spontaneous formation of a β-sheet nucleus, the above results support a two-stage process wereby aggregation and the initial formation of intermolecular hydrogen bonds occur rapidly (at least, at the concentration considered, 0.033 mol/L), but the reorganization of this network is a slow process characterized by a competition between β-sheet-like and nonspecific hydrogen bonds, as evidenced by the chaotic process depicted for aqueous aggregates in Figure 9(C). Reorganization is slowed down by the large number of disordered conformations, which act as kinetic traps along the path to an ordered, water-excluding core. This finding is consistent with a recent spectroscopic study suggesting that the rearrangement of early-stage oligomers via fragmentation, that is, breakage and reforming of interactions between peptide chains, plays an important role in the kinetics of amyloid formation.[91] Although we cannot discount the possibility that a β-sheet aggregate is not the stable endpoint of our system, self organization is apparent in the fact that β-sheet content reaches significant proportions over the course of the simulation [Fig. 9(D)].

Based on this study, the process of nucleation and propagation commonly assumed to be the mechanism of amyloid formation *in vitro* no longer applies when the monomers are bound to a hydrophobic surface. Catalysis of β-sheet formation occurs because each adsorbed monomer acts as a β-sheet primer, obviating the need for the formation of a nucleus and eliminating the rate-limiting step of aqueous amyloidogenesis. Self-organization is preceded by binding to the interface and conformational rearrangement of peptide monomers. Both hairpin-like and strand-like conformers favored by adsorption constitute templates for the formation of a β-sheet. Subsequently, monomers encounter each other through two-dimensional diffusion and readily form β-sheets. This mechanism is altogether different from a nucleation-propagation process, as there is no need for slow and extensive reorganization of the aggregate to reach a transient state with low propensity (the nucleus)

from which β-sheet evolves. As a result, the lag phase attributed to the rate-limiting nucleation step is entirely avoided. Instead, initial contact leads to partially formed β-sheets, whose subsequent reorganization is limited to maximizing the number of hydrogen bonds through the systematic elongation and improved registration of monomers. These findings are qualitatively consistent with a previous theoretical study which suggested that increasing the stability of a "β-prone" conformation allows the lag phase to be bypassed.[43]

Recent theoretical studies considered two limiting kinetic pathways of aqueous amyloidogenesis depending on β-sheet propensity and/or concentration.[46,48] In the high-propensity or low-concentration limit, the rate-limiting step is the addition of a monomer to ordered oligomers, whereas at high concentrations or low propensities, it is the extensive reorganization of disordered aggregates. As discussed above, our results in water are consistent with the latter mechanism. In contrast, the biphasic interface induces a mechanism of linear extension consistent with the high-propensity limit, since any monomer is a β-sheet template. Accordingly, most hydrogen bonds lead to β-sheets and the need for reorganization is limited even at high concentrations. It should be noted that the concentrations of peptides in our simulations of aggregation are orders of magnitude greater than those used for *in vitro* kinetics measurements, even in our low-concentration simulations B1 and B2. Nonetheless, the lifetime of peptide monomers is long enough to displace the conformational equilibrium of the polypeptide chain toward locally elongated conformations. Together, these results suggest that at low peptide concentrations, two-dimensional diffusion at the interface is the rate-limiting step not only for self-aggregation but also for self-organization.

In our simulations, we modeled the limits of high aqueous concentration and/or slow diffusion at the interface relative to water by allowing aggregation to occur prior to contact with the interface. Upon contact, the spontaneous partition of nonpolar side-chains into the octane phase forced the rapid reorganization of the disordered aggregate from 3D to 2D morphology, and the aggregate subsequently rearranged into β-sheets in a process similar to that observed following 2D diffusion of adsorbed monomers (Fig. 13). These results indicate that adsorption has the same organizing and catalyzing effect on β-sheet formation, regardless of the initial aggregation state of the peptides.

The three distinct pathways of peptide self-organization into β-sheets observed in this study are summarized in Figure 14. The only concentration-dependent step in the aqueous system is the aggregation of peptides into oligomers via 3D diffusion. In the biphasic system, two concentration-dependent steps are found at low concentration: 3D diffusion leading to peptide adsorption and 2D diffusion on the surface leading to aggregation (Fig. 14, top). At high aqueous concentration and/or slow surface diffusion, aqueous diffusion governs both aggrega-

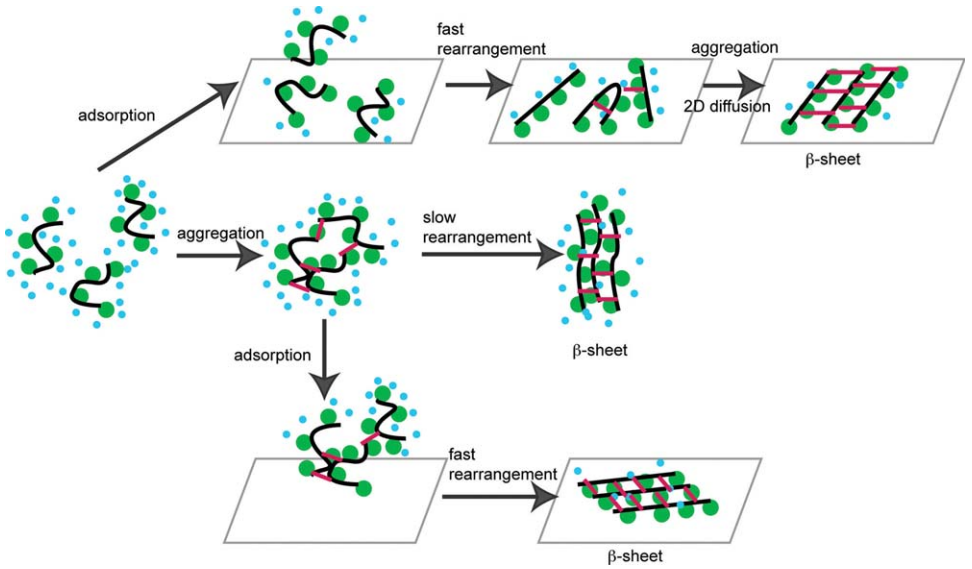

Figure 14

Schematic depiction of the effect of water-hydrophobic interfaces on the mechanism and kinetics of β-sheet formation. The peptide backbone (black), nonpolar side chains (green), water molecules (blue), and backbone–backbone hydrogen bonds (red) are shown together with the interface (gray). In water, the formation of disordered aggregates is followed by slow, extensive conformational reorganization (middle row). At low concentrations, adsorption of peptide monomers leads to their preorganization, which is followed by aggregation and limited reorganization (top). At high concentrations, adsorption of preformed, amorphous aqueous aggregates at the interface catalyzes their conformational reorganization into β-sheets (bottom).

tion and adsorption, and the rapid preorganization of peptide monomers is replaced by a rapid change in the morphology of the aggregate (Fig. 14, bottom). Thus, the interface catalyzes both pre and reorganization of the polypeptide chains. In both cases, the slow reorganization step limiting the rate of self-organization in aqueous aggregates is eliminated.

General implications to β-sheet formation in amyloidogenesis and protein folding

Amyloid formation in simple biphasic systems

This study offers a molecular explanation for the effect of hydrophobic interfaces on β-sheet formation by peptide aggregates, suggesting a generic mechanism for the catalysis of peptide self-organization resulting from phase separation of nonpolar side chains. Experimental studies of protein aggregation have shown that recombinant spider silk proteins form β-sheets at the air-water interface,[33] which also promotes the formation of β-sheet monolayers by lipopeptides containing amphipathic Leu-Glu repeats.[32] Air-water interfaces created by stirring were also demonstrated to accelerate *in vitro* amyloidogenesis.[34] Fibril formation was shown to be catalyzed by nanoparticles, with Trp side chains adsorbed on nonpolar surfaces.[28,29] Likewise, the treatment of α-synuclein with hexane granules increases the rate of formation of amyloid fibrils[27] and reverse micelles seed the formation of amyloid from Aβ-derived peptides.[26] Furthermore, nonpolar droplets increase aggregation of Aβ, although the aggregates formed in this way have a different morphology from those formed in water.[30] This study suggests a molecular mechanism for these observations, with the nonpolar phase acting as a template increasing the β-sheet propensity of the polypeptide chains, similar to the effect of the octane-water interface on our model peptides. The generality of this mechanism is corroborated by the fact the air-water interface also displaced the conformational equilibrium of $(GV)_4$ peptides toward β-prone conformations.

Our results are consistent with previous computational studies in which the conformational basis of aggregation was either not considered[56,87,88] or not reported.[92] As discussed above, coarse-grained simulations of peptide aggregation on the surface of nanoparticles[88] and lipid vesicles[87] captured the concentration effect resulting from surface binding. However, the low structural resolution of these models precludes a detailed examination of the physico-chemical basis of fibril formation. To model the effect of surface adsorption on the conformational equilibrium of peptides and proteins, the stereochemistry of the polypeptide backbone and side chains must be accounted for. In addition, it is unclear that the balance of various entropic effects and the essential role of side-chain and backbone dehydration in the mechanism of adsorption and self-organization, as uncovered in this study, would be attained with implicit representation of the solvent.

Two recent atomistic simulation studies have suggested that consistent with the present findings, orientational restriction is one of the primary effect of adsorption at hydrophobic interfaces.[56,92] In one of these studies, the effect of model hydrophilic and hydrophobic surfaces (including liquid-vapor) on the aggregation of hydrophilic and hydrophobic peptides was examined.[92] Only when both the surface and the peptides were hydrophobic did the peptides adsorb on the surface, where an increase in peptide aggregation relative to bulk water was interpreted in terms of increases in both concentration and orientational ordering.[92] In the other study, the dehydration of nonpolar side chains drove the partition of an amphipathic duodecapeptide monomer at the air-water interface and it was noted that such preorganization of monomers could facilitate self-organization into two-dimensional aggregates.[56] Reversible folding into a β-hairpin conformation occured and this conformation was shown to predominate both in bulk water and at the interface.[56] However, the later result does not imply that interfacial partition has not effect on the conformational equilibrium of the peptide: our study shows little difference in the population of hairpin-like conformations of $(GV)_4$ monomers in water and at the interface (Table II), although partition displaced the population of other (disordered and extended) conformational states.

Catalysis of amyloid formation at lipid-water interfaces

Like simple hydrophobic surfaces, lipid-water interfaces also catalyze amyloid formation.[18–25,93] Although this study constitutes a step toward understanding the molecular basis governing the interaction of amyloidogenic oligomers with lipid membranes, the octapeptides $(GA)_4$ and $(GV)_4$ have idealized sequences and octane only approximates biological interfaces. Here, we consider how the lipid-water interface and the amino-acid sequence may affect thermodynamic and kinetic properties of adsorption and self aggregation.

Our results indicate that nonpolar surfaces displace the conformational equilibrium of simple amyloidogenic peptides to conformational states prone to form extended β-sheets. The primary difference between lipid bilayers and the octane-water interface is the presence of a thick and chemically diverse interfacial region containing the polar and charged headgroups of lipids. This difference may in principle modulate the binding affinity of peptide side chains compared to that occurring at the octane-water interface due to coulombic interactions with polar and charged groups of the peptide. Different binding modes at the lipid-water interface may have different effects on the conformational equilibrium than observed in this study. In addition, the kinetics of aggregation is

likely to be affected by the longer relaxation scales[66] resulting from such interactions.

Consistent with this study, molecular simulation studies of the adsorption of peptide and amino acid analogues into lipid bilayers show that nonpolar side chains partition into the hydrophobic core of lipid membranes[85,94,95] and amphipathic peptides partition at the interface.[96–98] As discussed above, our results show that the octane-water interface is a quantitative model of the lipid-water interface in terms of adsorption of hydrophobic side chains, suggesting that the competing forces keeping amphipathic peptides on the surface of lipid bilayers are adequately modeled by the octane-water interface. Thus, our findings should extend to the lipid-water interface for sequences characterized by the alternance of polar and nonpolar residues, consistently with the fact that such sequences are strongly amyloidogenic.[99] Nonetheless, the long relaxation time scales of molecular motion at the lipid-water interface are likely to slow down the rates of adsorption, conformational rearrangement, and peptide aggregation relative to those observed at the octane-water interface.

To the extent that amyloid formation is driven by the hydrophobic effect, the molecular mechanism for the catalysis of β-sheet self-organization uncovered in this study is likely to play a role in the acceleration of amyloid formation by lipid bilayers. However, the significance of this effect for a given amino acid sequence should ultimately depend upon the extent to which the conformational equilibrium of the peptide is displaced toward elongated, β-prone conformations rather than other conformations such as α-helices (for example, other types of amphipathic sequences may form helices at the interface, whereas more uniformly nonpolar sequences may insert into the membrane[100,101]). Significant population of off-pathway conformational states would likely slow the kinetics of β-sheet self-organization. The detailed investigation of these effects will be the object of forthcoming studies. To this date, two studies have attempted to characterize the conformational equilibrium of an amyloidogenic peptide in a lipid bilayer. Replica-exchange MD simulations were used to examine the effect of lipid adsorption on the structure of the Aβ(1-42)[53,59] and Aβ(1-40) monomers.[59] In both studies, the peptides resided at the phospholipid interface. In one study, the Aβ(1-42) peptide adopted more extended conformations and transiently formed β-hairpins, but the authors concluded that it was more disordered than in aqueous solution.[53]

Protein folding

The mechanism of formation of amphipathic β-sheets uncovered above may be relevant to β-sheet formation on the surface of globular proteins. In as much as the hydrophobic effect drives protein folding,[102–104] the biphasic system considered in this study may be viewed as a model for the phase separation of polar and nonpolar residues inherent in the fold of globular domains. Our results suggest that, upon hydrophobic collapse, the partition of nonpolar side chains out of the aqueous phase may bias specific segments of the polypeptide chain with suitably amphipathic patterns to adopt locally elongated conformations comprising turns and strand-like conformations, restricting their conformational freedom and presenting partially dehydrated backbone amide groups to the vicinity of other strands; and that this process initiates the formation of β-sheets.

This model is consistent with the recognition that secondary structure elements in globular proteins are governed not only by the inherent preference of individual residues for a given type of structure (such as helix or strand), but also, essentially, by patterns of hydrophobic residues along the primary sequence, and that it is these patterns that determine the topology of the folded state.[103] Accordingly, amphiphilic sequences are found in solvent-exposed β-sheets of folded proteins and have been shown to form amyloid fibrils.[99] This analysis resonates with the facts that β-sheet propensity is modulated by tertiary context,[2,3] that most β-sheets of globular proteins are on the surface,[105] and most significantly, with the discovery that the single most important factor in the prediction of β-sheets is the formation of a nonpolar face.[1]

If the set of 20 naturally occuring amino acids is partitioned into polar and nonpolar residues, the most common patterns of amino acid polarity observed in the β-sheets of globular proteins have alternating polar and nonpolar residues (i.e., a periodicity of two).[105] However, this preference disappears when the sets are restricted to strongly polar (K, R, E, D, S, T, Q, N) and strongly hydrophobic residues (V, L, I, F, M), respectively.[106] The selection against *npnpnp* sequence periodicity, despite the inherent β-sheet preference for such patterns, is thought to reflect the need for avoiding amyloid. The recognition that proteins have evolved this trait to avert the amyloid fate is consistent with various strategies of "negative design".[99,107] Nevertheless, a recent analysis of sequence patterns using a restrictive subset of polar and nonpolar residues noted the presence of (i, i+2) nonpolar side-chain correlations at the N-terminus of parallel sheets and both N and C termini of antiparallel sheets in globular proteins.[106] The preference for alternating stretches at the end of β-sheet segments supports a mechanism whereby, consistent with this study, phase separation of amphipathic stretches initiates the formation of β-sheets.[106]

By extension, the present results also suggest that a similar mechanism could be involved in the early stages of forming β-barrels in integral membrane proteins, many of which are amphipathic as they possess a polar interior and present a nonpolar surface to the membrane

core.[108] In this process, the selective partition of nonpolar side chains into the hydrophobic phase may conceivably promote β-sheet nucleation on the lipid surface prior to the insertion and full formation of the barrel in the core of the lipid membrane.

SUMMARY AND CONCLUSION

We have used molecular dynamics simulations to examine the role of a nonpolar interface in the self-assembly of peptides into β-sheets. We have characterized the structural equilibrium and the aggregation properties of two simple octapeptides, $(GA)_4$ and $(GV)_4$, successively in aqueous solution and in the presence of a membrane-mimetic octane phase. Our results reveal that the mechanism and kinetics of aggregation at the biphasic interface differ dramatically from the expectations set out by the nucleation-propagation model and provide a simple molecular mechanism for the catalysis of amyloidogenesis by hydrophobic interfaces.

The preliminary step to β-sheet formation is the partition of the nonpolar side chains into the hydrophobic phase. This phase separation leaves the backbone lying at the interface, displaces the conformational equilibrium of the peptides toward locally extended, β-prone conformations, and induces partial dehydration of the polypeptide backbone, which favors the formation of intra and intermolecular peptide–peptide hydrogen bonds. As a result, once adsorbed monomers encounter each other through 2D diffusion, they readily form intermolecular hydrogen bonds and rapidly evolve β-sheet structure. In this process, displacement of the conformational equilibrium of the peptide monomer eliminates the need for a rate-limiting nucleation phase, since both the hairpin-like and strand-like conformations favored by adsorption provide templates for the formation of a β-sheet. Relative to aqueous aggregation, the nonpolar phase accelerates both the preorganization of peptide monomers and the reorganization of preformed aqueous aggregates.

Catalysis of β-sheet formation at the interface results from the interplay of four entropic factors, which are missing in the process of aqueous aggregation: the hydrophobic effect drives adsorption, which leads to an increase in concentration and to loss of orientational and conformational freedom. In this process, the biphasic nature and two-dimensional character of the interface complement those of β-sheets. Thus, the (entropic) catalysis of β-sheet self-organization by the water-hydrophobic interface results from the provision of a template whose two-dimensional topology and physical properties mirror those of amphipathic β-sheets.

The key finding of this study is the profound effect of interfacial adsorption on the conformational equilibrium of the peptides. Whether or not the present mechanism applies to more complex sequences should depend on the extent to which the conformational equilibrium of the peptides is displaced toward elongated conformations, rather than toward other conformations resulting in different degrees of insertion, different aggregation propensities, or different types of aggregates. It is reasonable to expect that both the primary sequence of the protein and polar interactions between protein and lipid headgroups play a role in this process—as suggested, for example, by the fact that amyloid catalysis is strongest with anionic lipids.[13,23–25] The modulation of aggregation properties by more complex sequences and by lipid interfaces of various composition will form the basis of forthcoming studies.

Although more work is needed to elucidate the molecular basis of membrane-protein interactions in the pathology of amyloid diseases, the generality of our findings extends beyond the catalysis of amyloid formation by hydrophobic interfaces. The results uncovered in this study suggest a generic mechanism of β-sheet formation, whereby the emergence of β-prone conformations upon phase-separation into a hydrophobic core precedes the formation of β-sheets not only in amyloidogenesis, but also in the folding of globular proteins and of integral membrane-bound β-barrels into their native state. In support of such a generic mechanism of β-sheet formation in protein folding, the formation of a nonpolar face has been found to be the single best predictor of β-sheet structure in globular proteins,[1] where this type of secondary structure often appears on the protein's surface.[105]

ACKNOWLEDGMENTS

This work was made possible by the Centre for Computational Biology at the Hospital for Sick Children, the facilities of the Shared Hierarchical Academic Research Computing Network (SHARCNET, www.sharcnet.ca), and Compute/Calcul Canada. This work was supported by HSF fellowship to SB, and an NSERC CGS scholarship to SR. RP is a CRCP chairholder.

REFERENCES

1. Parisien M, Major F. Ranking the factors that contribute to protein β-sheet folding. Proteins 2007;68:824–829.
2. Minor DL, Kim PS. Context is a major determinant of β-sheet propensity. Nature 1994;371:264–267.
3. He MM, Wood ZA, Baase WA, Xiao H, Matthews BM. Alanine-scanning mutagenesis of the b-sheet region of T4 lysozyme suggests that tertiary context has a dominant effect on β-sheet propensity. Protein Sci 2004;13:2716–2724.
4. Dobson CM. Protein folding and misfolding. Nature 2003;426: 884–890.
5. Chiti F, Dobson CM. Protein misfolding, functional amyloid, and human disease. Annu Rev Biochem 2006;75:333–366.
6. Jiménez JL, naki Guijarro JI, Orlova E, Zurdo J, Dobson CM, Sunde M, Saibil HR. Cryo-electron microscopy structure of an SH3 amyloid fibril and model of the molecular packing. EMBO J 1999;18:815–821.

7. Serpell LC, Blake CCF, Fraser PE. Molecular structure of a fibrillar Alzheimer's Aβ fragment. Biochemistry 2000;39:13269–13275.
8. Nelson R, Sawaya MR, Balbirnie M, Madsen AO, Riekel C, Grothe R, Eisenberg D. Structure of the cross-beta spine of amyloid-like fibrils. Nature 2005;435:773–778.
9. Jahn TR, Makin OS, Morris KL, Marshall KE, Tian P, Sikorski P, Serpell LC. The common architecture of cross-β amyloid. J Mol Biol 2010;395:717–727.
10. Sawaya MR, Sambashivan S, Nelson R, Ivanova MI, Sievers SA, Apostol MI, Thompson MJ, Balbirnie M, Wiltzius JJW, McFarlane HT, Madsen AØ, Riekel C, Eisenberg D. Atomic structures of amyloid cross-β spines reveal varied steric zippers. Nature 2007;447:453–457.
11. Wiltzius JJ, Sievers SA, Sawaya MR, Cascio D, Popov D, Riekel C, Eisenberg D. Atomic structure of the cross-β spine of Islet Amyloid Polypeptide (Amylin). Protein Sci 2008;17:1467–1474.
12. Vilar M, Chou HT, Luhrs T, Maji SK, Riek-Loher D, Verel R, Manning G, Stahlberg H, Riek R. The fold of {alpha}-synuclein fibrils. Proc Natl Acad Sci USA 2008;105:8637.
13. McLaurin JA, Chakrabartty A. Membrane disruption by Alzheimer beta-amyloid peptides mediated through specific binding to either phospholipids or gangliosides. J Biol Chem 1996;280:30001–30008.
14. Hebda JA, Miranker AD. The interplay of catalysis and toxicity by amyloid intermediates on lipid bilayers: insights from type II diabetes. Annu Rev Biophys 2009;38:125–152.
15. Volles MJ, Lee SJ, Rochet JC, Shtilerman MD, Ding TT, Kessler JC, Lansbury PT, Jr. Vesicle permeabilization by protofibrillar α-synuclein: implications for the pathogenesis and treatment of Parkinson's disease. Biochemistry 2001;40:7812–7819.
16. Zhu M, Fink AL. Lipid binding inhibits alpha-synuclein fibril formation. J Biol Chem 2003;278:16873–16877.
17. Pastor MT, Kümmerer N, Schubert V, Esteras-Chopo A, Dotti CG, López de la Paz M, Serrano L. Amyloid toxicity is independent of polypeptide sequence, length, and chirality. J Mol Biol 2008; 375:695–707.
18. Lee HJ, Choi C, Lee SJ. Membrane-bound α-synuclein has a high aggregation propensity and the ability to seed the aggregation of the cytosolic form. J Biol Chem 2002;277:671–678.
19. Jo E, McLaurin JA, Yip CM, St. George-Hyslop P, Fraser PE. α-Synuclein membrane interactions and lipid specificity. J Biol Chem 2000;275:34328–34334.
20. Valincius G, Heinrich F, Budvytyte R, Vanderah DJ, Sokolov Y, Hall JE, Lösche M. Soluble amyloid β-oligomers affect dielectric membrane properties by bilayer insertion and domain formation: implications for cell toxicity. Biophys J 2008;95:4845–4861.
21. Sparr E, Engel MFM, Sakharov DV, Sprong M, Jacobs J, de Kruijff B, Höppener JWM, Killian JA. Islet amyloid polypeptide-induced membrane leakage involves uptake of lipids by forming amyloid fibers. FEBS Lett 2004;577:117–120.
22. Canale C, Torrassa S, Rispoli P, Relini A, Rolandi R, Bucciantini M, Stefani M, Gliozzi A. Natively folded HypF-N and its early amyloid aggregates interact with phospholipid monolayers and destabilize supported phospholipid bilayers. Biophys J 2006; 91:4575.
23. Zhao H, Tuominen EKJ, Kinnunen PKJ. Formation of amyloid fibers triggered by phosphatidylserine-containing membranes. Biochemistry 2004;43:10302–10307.
24. Zhu M, Souillac PO, Ionescu-Zanetti C, Carter SA, Fink AL. Surface-catalyzed amyloid fibril formation. J Biol Chem 2002;277: 50914–50922.
25. Yip CM, Darabie AA, McLaurin JA. Abeta-peptide assembly on lipid bilayers. J Mol Biol 2002;318:97–107.
26. Mukherjee S, Chowdhury P, Gai F. Effect of dehydration on the aggregation kinetics of two amyloid peptides. J Phys Chem B 2009;113:531–535.
27. Lee J, Bhak G, Lee SG, Paik SR. Instantaneous amyloid fibril formation of α-synuclein from the oligomeric granular structures in the presence of hexane. Biophys J 2008;95:L16–L18.
28. Linse S, Cabaleiro-Lago C, Xue WF, Lynch I, Lindman S, Thulin E, Radford SE, Dawson KA. Nucleation of protein fibrillation by nanoparticles. Proc Natl Acad Sci USA 2007;104:8691–8696.
29. Colvin VL, Kulinowski KM. Nanoparticles as catalysts for protein fibrillation. Proc Natl Acad Sci USA 2007;104:8679–8680.
30. Nichols MR, Moss MA, Reed DK, Hoh JH, Rosenberry TL. Rapid assembly of amyloid-beta peptide at a liquid/liquid interface produces unstable beta-sheet fibers. Biochemistry 2005;44:165–173.
31. Schladitz C, Vieira EP, Hermel H, Möhwald H. Amyloid-β-sheet formation at the air-water interface. Biophys J 1999;77:3305–3310.
32. Cavalli S, Handgraaf JW, Tellers EE, Popescu DC, Overhand M, Kjaer K, Vaiser V, Sommerdijk NA, Rapaport H, Kros A. Two-dimensional ordered β-sheet lipopeptide monolayers. J Am Chem Soc 2006;128:13959–13966.
33. Renault A, Rioux-Dubé JF, Lefèvre T, Pezennec S, Beaufils S, Vié V, Tremblay M, Pézolet M. Surface properties and conformation of Nephila clavipes spider recombinant silk proteins at the air-water interface. Langmuir 2009;25:8170–8180.
34. Jean L, Lee CF, Lee C, Shaw M, Vaux DJ. Competing discrete interfacial effects are critical for amyloidogenesis. FASEB J 2010; 24:309–317.
35. Stefani M. Protein folding and misfolding on surfaces. Int J Mol Sci 2008;9:2515–2542.
36. Hall CK, Wagoner VA. Computational approaches to fibril structure and formation. Meth Enzymol 2006;412:338–365.
37. Ma J, Nussinov R. Simulations as analytical tools to understand protein aggregation and predict amyloid conformation. Curr Opin Chem Biol 2006;10:445–452.
38. Jang S, Shin S. Computational study of the structural diversity of amyloid beta peptide ($A\beta_{10\text{-}35}$) oligomers. J Phys Chem B 2008; 112:3479–3484.
39. López de la Paz M, de Mori M, Serrano L, Colombo G. Sequence dependence of amyloid fibril formation: insights from molecular dynamics simulations. J Mol Biol 2005;349:583–596.
40. Gnanakaran S, Nussinov R, García AE. Atomic-level description of amyloid beta-dimer formation. J Am Chem Soc 2006;128:2158–2159.
41. Urbanc B, Cruz L, Ding F, Sammond D, Khare S, Buldyrev SV, Stanley HE, Dokholyan . Molecular dynamics simulation of amyloid β dimer formation. Biophys J 2004;87:2310–2321.
42. Nguyen HD, Hall CK. Molecular dynamics simulations of spontaneous fibril formation by random-coil peptides. Proc Natl Acad Sci USA 2004;101:16180–16185.
43. Pellarin R, Caflisch A. Interpreting the aggregation kinetics of amyloid peptides. J Mol Biol 2006;360:882–892.
44. Pellarin R, Guarnera E, Caflisch A. Pathways and intermediates of amyloid fibril formation. J Mol Biol 2007;374:917–924.
45. Marchut AJ, Hall CK. Effects of chain length on the aggregation of model polyglutamine peptides: molecular dynamics simulations. Proteins 2007;66:96–109.
46. Auer S, Dobson CM, Vendruscolo M. Characterization of the nucleation barriers for protein aggregation and amyloid formation. HFSP J 2007;1:137–146.
47. Bellesia G, Shea JE. Effect of β-sheet propensity on peptide aggregation. J Chem Phys 2009;130:145103.
48. Bellesia G, Shea JE. Diversity of kinetic pathways in amyloid fibril formation. J Chem Phys 2009;131:111102.
49. Wu C, Lei H, Duan Y. The role of Phe in the formation of well-ordered oligomers of amyloidogenic hexapeptide (NFGAIL) observed in molecular dynamics simulations with explicit solvent. Biophys J 2005;88:2897–2906.
50. Gsponer J, Haberthur U, Caflisch A. The role of side-chain interactions in the early steps of aggregation: molecular dynamics simulations of an amyloid-forming peptide from the yeast prion Sup35. Proc Natl Acad Sci USA 2003;100:5154.
51. Han W, Wu YD. A strand-loop-strand structure is a possible intermediate in fibril elongation: long time simulations of amyloid-beta peptide. J Am Chem Soc 2005;127:15408–15416.

52. Davis CH, Berkowitz ML. Interaction between amyloid-beta (1-42) peptide and phospholipid bilayers: a molecular dynamics study. Biophys J 2009;96:785–797.
53. Davis CH, Berkowitz ML. Structure of the amyloid-b (1-42) monomer absorbed to model phospholipid bilayers: a molecular dynamics study. J Phys Chem B 2009;113:14480–14486.
54. Crowet JM, Lins L, Dupiereux I, Elmoualija B, Lorin A, Charloteaux B, Stroobant V, Heinen E, Brasseur R. In silico tilted properties of the 67-78 fragment of α-synuclein are responsible for membrane destabilization and neurotoxicity. Proteins 2007;68: 936–947.
55. Jang H, Zheng J, Nussinov R. Models of β-amyloid ion channels in the membrane suggest that channel formation in the bilayer is a dynamic process. Biophys J 2007;93:1938.
56. Knecht V. β-hairpin folding by a model amyloid peptide in solution and at an interface. J Phys Chem B 2008;112:9476–9483.
57. Lemkul JA, Bevan DR. A comparative molecular dynamics analysis of the amyloid β-peptide in a lipid bilayer. Arch Biochem Biophys 2008;470:54–63.
58. Lemkul JA, Bevan DR. Perturbation of membranes by the amyloid b-peptide—A molecular dynamics study. FEBS J 2009;276:3060–3075.
59. Miyashita N, Straub JE, Thirumalai D. Structures of beta-amyloid peptide 1-40, 1-42, and the 672-726 fragment of APP in a membrane environment with implications for interactions with gamma-secretase. J Am Chem Soc 2009;131:17843–17852.
60. Mobley DL, Cox DL, Singh RRP, Maddox MW, Longo ML. Modeling amyloid beta-peptide insertion into lipid bilayers. Biophys J 2004;86:3585–3597.
61. Xu Y, Shen J, Luo X, Zhu W, Chen K, Ma J, Jang H. Conformational transition of amyloid β-peptide. Proc Natl Acad Sci USA 2005;102:5403–5407.
62. Kenney JM, Knight D, Wise MJ, Vollrath F. Amyloidogenic nature of spider silk. FEBS J 2002;269:4159–4163.
63. Rathore O, Sogah DY. Nanostructure formation through β-sheet self-assembly in silk-based materials. Macromolecules 2001;34: 1477–1486.
64. Vandermeulen GWM, Kim KT, Wang Z, Manners I. Metallopolymer-peptide conjugates: synthesis and self-assembly of polyferrocenylsilane graft and block copolymers containing a β-sheet forming Gly-Ala-Gly-Ala tetrapeptide segment. Biomacromol 2006;7:1005–1010.
65. Rauscher S, Baud S, Miao M, Keeley FW, Pomès R. Proline and glycine control protein self-organization into elastomeric or amyloid fibrils. Structure 2006;14:1667–1676.
66. Tieleman DP, Berendsen HJC, Sansom MSP. Voltage-dependent insertion of alamethicin at phosholipid/water and octane/water interfaces. Biophys J 2001;80:331–346.
67. Stockner T, Ash WL, MacCallum JL, Tieleman DP. Direct simulation of transmembrane helix association: role of asparagines. Biophys J 2004;87:1650–1656.
68. Jorgensen WL, Maxwell DS, Tirado-Rives J. Development and testing of the OPLS all-atom force-field on conformational energetics and properties of organic liquids. J Am Chem Soc 1996;118: 11225–11236.
69. Jorgensen WL, Chandrasekhar J, Madura JD, Impey RW, Klein ML. Comparison of simple potential functions for simulating liquid water. J Chem Phys 1983;79:926.
70. Lindahl E, Hess B, van der Spoel D. GROMACS 3.0: a package for molecular simulation and trajectory analysis. J Mol Model 2001;7:306–317.
71. Berendsen HJC, van der Spoel D, van Drunen R. GROMACS: a message-passing parallel molecular dynamics implementation. Comp Phys Comm 1995;91:43–56.
72. Essmann U, Perera L, Berkowitz ML, Dardent T, Lee H, Pedersen LG. A smooth particle mesh Ewald method. J Chem Phys 1995;103:8577–8593.
73. Berendsen HJC, Postma JPM, van Gunsteren WF, DiNola A, Haak JR. Molecular dynamics with coupling to an external bath. J Chem Phys 1984;81:3684.
74. Hess B, Bekker H, Berendsen HJC, Fraaije JGEM. LINCS: a linear constraint solver for molecular simulations. J Comp Chem 1997;18:1463–1472.
75. Miyamoto S, Kollman PA. Settle: an analytical version of the SHAKE and RATTLE algorithm for rigid water models. J Comp Chem 1992;13:952–962.
76. Rodinger T, Howell PL, Pomès R. Distributed replica sampling. J Chem Theory Comput 2006;2:725–731.
77. Rodinger T, Howell PL, Pomès R. Calculation of absolute protein-ligand binding affinities using distributed replica sampling. J Chem Phys 2008;129:155102.
78. Rauscher S, Neale C, Pomès R. Simulated tempering distributed replica sampling, virtual replica exchange, and other generalized-ensemble methods for conformational sampling. J Chem Theory Comput 2009;5:2640–2662.
79. Nosé S. A molecular-dynamics method for simulations in the canonical ensemble. Mol Phys 1984;52:255–268.
80. Hoover WG. Canonical dynamics–equilibrium phase-space distributions. Phys Rev A 1985;31:1695–1697.
81. Pandit SA, Bostick D, Berkowitz ML. An algorithm to describe molecular scale rugged surfaces and its application to the study of a water/lipid bilayer interface. J Chem Phys 2003;119:2199.
82. Kabsch W, Sander C. Dictionary of protein secondary structure: pattern recognition of hydrogen-bonded and geometrical features. Biopolymers 1983;22:2577–2637.
83. Allen MP, Tildesley DJ. Computer Simulation of Liquids. Clarendon Press; Oxford 1987.
84. Radzicka A, Wolfenden R. Comparing the polarities of the amino acids: side-chain distribution coefficients between the vapor phase, cyclohexane, 1-octanol, and neutral aqueous solution. Biochemistry 1988;27:1664–1670.
85. MacCallum JL, Bennett WF, Tieleman DP. Partitioning of amino acid side chains into lipid bilayers: results from computer simulations and comparison to experiment. J Gen Physiol 2007;129:371–377.
86. Wimley WC, Creamer TP, White SH. Solvation energies of amino acid side chains and backbone in a family of host-guest pentapeptides. Biochemistry 1996;35:5109–5124.
87. Friedman R, Pellarin R, Caflisch A. Amyloid aggregation on lipid bilayers and its impact on membrane permeability. J Mol Biol 2009;378:407–415.
88. Auer S, Trovato A, Vendruscolo M. A condensation-ordering mechanism in nanoparticle-catalyzed peptide aggregation. PLoS Comput Biol 2009;5:e1000458.
89. Chiti F, Dobson CM. Protein misfolding, functional amyloid, and human disease. Annu Rev Biochem 2006;75:333–336.
90. Murphy RM. Kinetics of amyloid formation and membrane interaction with amyloidogenic proteins. Biochim Biophys Acta 2007;1768:1923–1934.
91. Xue W-F, Homans SW, Radford SE. Systematic analysis of nucleation-dependent polymerization reveals new insights into the mechanism of amyloid self-assembly. Proc Natl Acad Sci USA 2008;105:8926–8931.
92. Brovchenko I, Singh G, Winter R. Aggregation of amyloidogenic peptides near hydrophobic and hydrophillic surfaces. Langmuir 2009;25:8111–8116.
93. Sharp JS, Forrest JA, Jones RAL. Surface denaturation and amyloid fibril formation of insulin at model lipid-water interfaces. Biochemistry 2002;41:15810–15819.
94. MacCallum JL, Bennett WF, Tieleman DP. Distribution of amino acids in a lipid bilayer from computer simulations. Biophys J 2008;94:3393–3404.
95. Johansson AC, Lindahl E. Position-resolved free energy of solvation for amino acids in lipid membranes from molecular dynamics simulations. Proteins 2008;70:1332–1344.

96. Khandelia H, Ipsen JH, Mouritsen OG. The impact of peptides on lipid membranes. Biochim Biophys Acta 2008;1778:1528–1536.
97. Matyus E, Kandt C, Tieleman DP. Computer simulation of antimicrobial peptides. Curr Med Chem 2008;14:2789–2798.
98. Aliste MP, Tieleman DP. Computer simulation of partitioning of ten pentapeptides Ace-WLXLL at the cyclohexane/water and phospholipid/water interfaces. BMC Biochem 2005;6:30.
99. Broome BM, Hecht MH. Nature disfavors sequences of alternating polar and non-polar amino acids: implications for amyloidogenesis. J Mol Biol 2000;296:961–968.
100. White SH, Wimley WC. Membrane protein folding and stability: physical principles. Annu Rev Biophys Biomol Struct 1999;28:319–365.
101. Hessa T, Kim H, Bihlmaier K, Lundin C, Boekel J, Andersson H, Nilsson I, White SH, von Heijne G. Recognition of transmembrane helices by the endoplasmic reticulum translocon. Nature 2005;433:377–381.
102. Kauzmann W. Some factors in the interpretation of protein denaturation. Adv Prot Chem 1959;14:1–63.
103. Rose GD, Roy S. Hydrophobic basis of packing in soluble proteins. Proc Natl Acad Sci USA 1980;77:4643–4647.
104. Dill KA, Fiebig KM, Chan HS. Cooperativity in protein-folding kinetics. Proc Natl Acad Sci USA 1993;90:1942–1946.
105. Mandel-Gutfreund Y, Gregoret LM. On the significance of alternating patterns of polar and non-polar residues in β-strands. J Mol Biol 2002;323:453–461.
106. Wathen B, Jia Z. Folding by numbers: primary sequence statistics and their use in studying protein folding. Int J Mol Sci 2009;10:1567–1589.
107. Monsellier E, Chiti F. Prevention of amyloid-like aggregation as a driving force of protein evolution. EMBO Rep 2007;8:737–742.
108. Tamm LK, Hong H, Liang B. Folding and assembly of β-barrel membrane proteins. Biochim Biophys Acta 2004;1666:250–263.